Charged colloids near interfaces



2001 J. Phys.: Condens. Matter 13 4801

(http://iopscience.iop.org/0953-8984/13/21/311)

INSTITUTE OF PHYSICS PUBLISHING JOURNAL OF PHYSICS: CONDENSED MATTER

J. Phys.: Condens. Matter **13** (2001) 4801–4834 www.iop.org/Journals/cm PII: S0953-8984(01)19851-6

# Charged colloids near interfaces

**H H von Grünberg and E C Mbamala**

Fakultät für Physik, Universität Konstanz, 78457 Konstanz, Germany

Received 7 December 2000, in final form 23 January 2001

**Abstract**

This article deals with the electric double-layer force between a charged colloidal sphere and a charged dielectric planar wall. To introduce the problem and to uncover the basic physics involved, we start by first reviewing the effective wall–colloid potentials that one obtains in linearized Poisson–Boltzmann theory. The important key concepts in this context are: charge renormalization, confinement effects, salty interfaces, and image-charge effects due to the dielectric discontinuity at the wall. Starting from the potentials derived in linear theory, we then come to approximate wall–colloid potentials that are valid also in the parameter regime where the non-linearity of the Poisson–Boltzmann equation becomes important. The range of validity of these potentials is systematically investigated by comparing them with potentials based on the exact numerical solution to the Poisson–Boltzmann equation. The important parameters of the calculation are the salt content of the electrolytic solution, the colloidal sphere radius, and the surface charge densities on both the wall and the colloid. We then briefly discuss what additional effect a concentrated suspension of such colloidal spheres has on the interfacial colloid, and close with a short report of an optical experiment that has recently been performed to measure the approximate wall–colloid potentials investigated here.

## 1. Introduction

This article is concerned with the apparently simple question of how a charged colloidal sphere inside an electrolytic solution interacts with a planar wall which has a dielectric constant that is different from that of the solution and which may or may not bear any surface charges. That this is, in fact, a rather complicated question, containing many theoretically interesting aspects, becomes obvious from the following list of observations:

(i) The fixed charges on both the colloidal sphere and the wall are screened by the salt ions of the solution; a layer of mobile ions of the electrolyte (double layer) forms near the interface and the colloidal sphere [1, 2]. The electrolyte ions of this double layer will readjust themselves in response to any change of the colloid–wall separation.

0953-8984/01/214801+34$30.00  

(ii) Any charged object near an interface between two media of different dielectric constants will experience a force due to induced polarization charges at the interface. This gives rise to image charges which add to the normal interfacial charges. Image charges have the same effect as real charges and will therefore affect the structure of the double layer.

(iii) The Poisson–Boltzmann (PB) equation governing the whole problem is a differential equation with a complicated non-linearity caused by exponential factors. It can only be solved numerically.

(iv) Even when we know the complex density distribution of small ions around and between the sphere and wall for every possible wall–colloid distance, we still have a long way to go: from this density distribution, one can obtain the grand potential of the system. This quantity, when seen as a function of the colloid–wall distance, can be regarded as the *effective* colloid–wall interaction potential where the term 'effective' is a reminder of the fact that an initial multi-component system has been reduced to a smaller system consisting of just the sphere and the wall. Such effective colloid–wall potentials are what we want to calculate in this article.

To show why the subject of this article, besides being interesting, is also of practical interest, we content ourselves with just recalling a few recent experiments where charged colloids (or biocolloids) near an interface play a major role. There are, first, a long series of optical experiments where the effective pair potentials between colloids near a glass surface have been measured, with the surprising finding that colloids may attract each other, even though they bear like charges [3]. This unexpected attraction has caused a long theoretical debate on whether or not this can be explained within the PB theory [4], and has only recently been consistently interpreted in terms of hydrodynamic interactions [5]. A second set of papers related to our problem are concerned with the adsorption of charged polyelectrolytes, specifically DNA molecules, on fluid or glass-supported cationic lipid bilayers [6], where image-charge effects might be of considerable importance [7]. We finally mention TIRM (total internal reflection microscopy), a new optical method based on the evanescent wave near an interface, designed to measure the interaction between a single colloidal particle and a wall [8], which in many respects can compete with more established methods for measuring forces such as methods using the surface force apparatus [9]. We will report on a TIRM experiment in the last section of this paper; another interesting example can be found in reference [10] where the effective interaction between a biological cell and a smooth surface has been studied using the TIRM method. Other works—and this list is by no means comprehensive—related to our subject of colloids near interfaces are studies of the structural properties of interfacial colloidal suspensions [11], wall-induced layering in colloidal hard-sphere glasses [12], and supercooled colloidal suspensions [13]; see also reference [14]. On the theoretical side, we mention a string of papers on image-charge effects on colloidal crystal ordering [15], the huge field of lipid–protein interaction—see for instance [16]—and older papers on colloidal aggregation [17] and melting [18] affected in some ways by walls.

We here solve the PB equation numerically to determine the mean-field electrostatic potential and, from it, the effective interaction potential between the colloid and the wall. We compare the numerically determined potentials with approximate analytical potentials and check systematically in what parameter region these potentials can be used. Carnie and co-workers (see e.g. references [19–24]) have made quite an extensive study of the interaction energy and force of two similar or dissimilar spheres in an electrolyte including recently [23] a sphere and a plate. In most of these studies, they have compared results obtained by numerical solution of the full PB equation with those from approximate models: the linear superposition approximation, the Derjaguin method, etc.

Warszynski and Adamczyk [25], also treating two dissimilar spheres and sphere/plate interaction, have gone a step further in their numerical scheme, to include the electric field distributions within the particles and plate (wall) which are usually neglected by most workers, as in the present paper. Bhattacharjee and Elimelech [26] used a method that they referred to as surface element integration to determine the van der Waals and electrostatic double-layer interaction between a particle (a sphere in particular) and an infinite plate, starting from the well-known energy of interaction between two infinite parallel plates. Their method, which basically integrates the flat-plate interaction energy per unit area over a planar projected area on the particle surface, seems to agree well with a numerical solution of the problem and improves on the conventional Derjaguin method.

In the three studies [23,25,26], the PB equation has been solved in the sphere/wall geometry and compared to approximate models that are often themselves based on numerical solutions. Our philosophy here is somewhat different: we take less sophisticated analytical potentials, to be found already in the classical book on colloids by Verwey and Overbeek [27], which have however the advantage of being more handy for experimentalists as they are of purely analytical form. This, in conjunction with the fact that we have systematically explored the range of validity of these potentials, should make this paper useful primarily to those who need a quick estimate of the wall–colloid interaction energy but not the best accuracy possible. Another feature of this paper might be seen in that we emphasize the role played by image charges and that, contrary to other studies [23, 25, 26], ours takes account of their contribution to the effective wall–colloid interaction potential, which results in a non-zero interaction even when the wall is uncharged.

The calculation based on the non-linear PB equation is presented in section 4. Since the purpose of the present paper is not only to present new results, but also to convey a more profound insight into the basic physics of the problem, we give in section 3 a detailed discussion of older works on the effective colloid–wall interaction based on the linearized PB theory. We begin with section 2 which is devoted to clarifying the concept of 'effective interactions'.

## 2. Exposition of the problem: the concept of effective interactions

We consider a charged spherical colloid in the vicinity of a planar interface between an electrolytic solution and a dielectric substrate. At this interface, there can be additional interfacial charges. The electrolyte is assumed to be unbounded; that is, there is a reservoir of electrolyte ions coupled to our system, so the number of ions in the system is not fixed. The thermodynamic variables that are fixed are thus: the temperature (given by $\beta = 1/kT$), the chemical potential of the salt ions $\mu_s$, and the volume $V$, so the ensemble that we work in is the grand-canonical ensemble with the grand potential $\Omega$ being the relevant thermodynamic potential. The principal question guiding us through this study then is: how does the grand potential of the whole system depend on the distance $h$ of the colloidal sphere from the interface? This function can be regarded as the effective colloid–wall interaction potential [28, 29].

Our strategy for calculating this effective potential is (i) to solve the mean-field PB equation [30] for a fixed colloid–wall distance $h$ to determine the electrostatic mean-field potential $\phi$, and (ii) to use this potential to evaluate the grand potential. Repeating this procedure for varying $h$, we then obtain the effective interaction potential as a function of $h$. Specifically, we have to solve the following PB equation for the normalized potential $\phi$:

$$\nabla^2\phi = \kappa^2 \sinh\phi \tag{1}$$

where $\phi = e\beta\psi$ with $\psi$ being the usual electrostatic potential and $e$ the elementary charge.

$\kappa^2 = 8\pi\lambda_B c_s$ is the screening parameter characterizing the electrolytic solution, $\lambda_B = e^2\beta/\epsilon$ is the Bjerrum length, and $\epsilon$ is the dielectric constant of the solvent. In our grand-canonical description, the bulk concentration $c_s$ of electrolyte ions (assumed to have a valency of one) is a fixed input parameter of the calculation, and is directly related to the chemical potential of the salt, $\beta\mu_s = \log c_s\Lambda^3$, with $\Lambda^3$ being the usual thermal wavelength. The local density of positive/negative salt ions can be obtained from $\rho_\pm = c_s e^{\mp\phi}$, so the net charge density at a given point $\vec{r}$ in the solution is $\rho(\vec{r}) = \rho_- - \rho_+$, and the ion number density is $n(\vec{r}) = \rho_- + \rho_+$.

The colloidal sphere of radius $a$ bears $Z$ negative surface charges, while the confining wall has a surface charge density of $-e\sigma_w$. These charges, which are *fixed* charges, in contrast to the salt ions which are *mobile* charges, enter the problem through the boundary conditions. Let us call the boundary given by the $z = 0$ interfacial wall $\partial G_w$, the surface of our colloid $\partial G_c$, the region of the electrolytic solution between the two surfaces $G$, and the negative $z < 0$ half-space $G_<$; see figure 1. At $\partial G_c$ we then require the normal component of the electric field to be identical to the colloidal surface charge density $\sigma_c = Z/4\pi a^2$ (the constant-charge boundary condition), while at $\partial G_w$ we must demand that the normal component of the electric displacement field jumps by the amount $4\pi\epsilon\lambda_B\sigma_w$. In addition, we assume that the dielectric constant of the colloid is zero and that the potential vanishes at infinity.

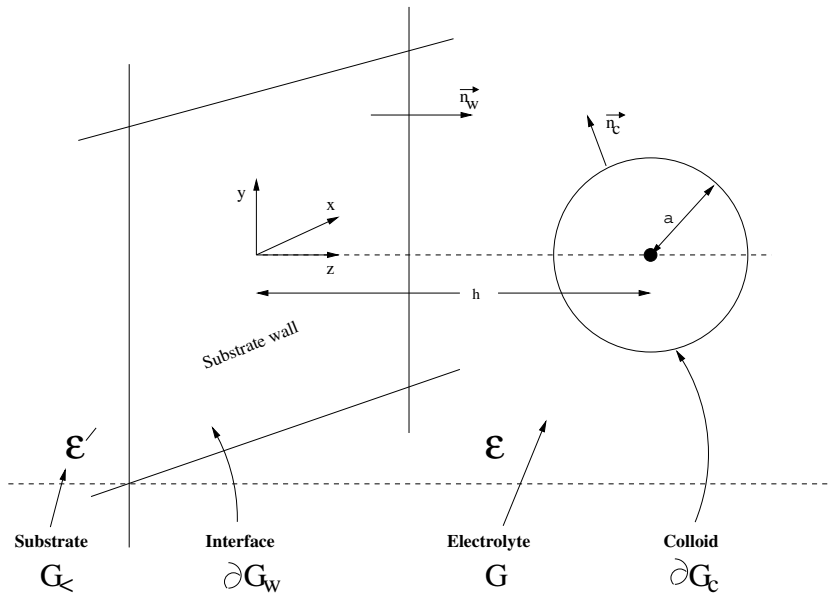


**Figure 1.** Our system: a colloid of charge $-Ze$ and radius $a$ inside an electrolytic solution of dielectric constant $\epsilon$, a distance $h$ away from a substrate of dielectric constant $\epsilon'$.

The PB equation, along with these boundary conditions, then leads to the following boundary value problem (BVP) for $\phi$:

$$\begin{aligned}
&\nabla^2\phi = \kappa^2 \sinh\phi && \vec{r} \in G \\
&\nabla^2\phi = 0 && \vec{r} \in G_< \\
&\epsilon\vec{n}_w \nabla\phi\big|_{z=0+} - \epsilon'\vec{n}_w \nabla\phi\big|_{z=0-} = 4\pi\epsilon\lambda_B\sigma_w && \vec{r} \in \partial G_w \\
&\vec{n}_c \nabla\phi = 4\pi\lambda_B\sigma_c && \vec{r} \in \partial G_c \\
&\phi = 0 && \text{at } \infty
\end{aligned} \tag{2}$$

where $\epsilon'$ is the dielectric constant of the substrate. $\vec{n}_w$ and $\vec{n}_c$ are two unit vectors directed normal to the surfaces of the wall and colloidal sphere, respectively, and pointing towards $G$. Since there is still rotational symmetry about the $z$-axis (see figure 1), equation (2) here is a differential equation in two spatial variables.

Once we know $\phi$, we can proceed to calculate the grand potential of our system:

$$\beta\Omega = \frac{1}{8\pi\lambda_B}\int_G \mathrm{d}\vec{r}\ (\nabla\phi)^2 + \frac{\epsilon'/\epsilon}{8\pi\lambda_B}\int_{G_<} \mathrm{d}\vec{r}\ (\nabla\phi)^2 + \sum_{\alpha=\pm}\int_G \mathrm{d}\vec{r}\ \rho_\alpha(\log\rho_\alpha\Lambda^3 - 1) - \beta\mu_s\int_G \mathrm{d}\vec{r}\ (\rho_+ + \rho_-) + \int_G \mathrm{d}\vec{r}\ 2c_s - \beta W^{SE}. \tag{3}$$

The first two terms give the energy stored in the electric field in $G$ and $G_<$, the third gives the entropy of mixing of the microions, and the fourth accounts for the fact that the number of ions in the system varies. The last term, $\beta W^{SE}$, is the energy of the $Z$ colloidal charges in their own Coulomb potential ($=Z^2\lambda_B/2a$ if $a$ is finite), a constant which we have subtracted for later convenience. On substitution of $\rho_\pm = c_s\mathrm{e}^{\mp\phi}$ and $\beta\mu_s = \log c_s\Lambda^3$, equation (3) becomes

$$\beta\Omega = \frac{1}{8\pi\lambda_B}\left[\int_G \mathrm{d}\vec{r}\ (\nabla\phi)^2 + \frac{\epsilon'}{\epsilon}\int_{G_<} \mathrm{d}\vec{r}\ (\nabla\phi)^2 + 2\kappa^2\int_G \mathrm{d}\vec{r}\ \big(\phi\sinh\phi - \cosh\phi + 1\big)\right] - \beta W^{SE}. \tag{4}$$

Using Green's first identity, we can decompose the terms $\int \mathrm{d}\vec{r}\ (\nabla\phi)^2$, so we have

$$\beta\Omega = \frac{1}{8\pi\lambda_B}\left[-\int_{\partial G_w}\mathrm{d}S\left[\vec{n}_w\,\nabla\phi\big|_{z=0+} - \frac{\epsilon'}{\epsilon}\vec{n}_w\,\nabla\phi\big|_{z=0-}\right]\phi - \int_{\partial G_c}\mathrm{d}S\,\vec{n}_c\,\nabla\phi\,\phi + \kappa^2\int_G \mathrm{d}\vec{r}\ (\phi\sinh\phi - 2\cosh\phi + 2)\right] - \beta W^{SE}. \tag{5}$$

This can be further simplified by inserting the boundary conditions of the BVP in equation (2), which leads to

$$\beta\Omega_h = -\frac{\sigma_w}{2}\int_{\partial G_w}\mathrm{d}S\,\phi_h - \frac{\sigma_c}{2}\int_{\partial G_c}\mathrm{d}S\,\phi_h + c_s\int_G \mathrm{d}\vec{r}\ (\phi_h\sinh\phi_h - 2\cosh\phi_h + 2) - \beta W^{SE}. \tag{6}$$

One should be aware of the fact that the position of the boundary $\partial G_c$ in equation (2) still depends on the colloid–wall distance $h$. Thus, for one specific value of the external parameter $h$, we have one BVP to solve. In equation (6), we therefore wrote $\phi_h$ to stress that $\phi$ still depends parametrically on $h$, and so does the grand potential. We can now define the effective wall–colloid interaction potential $\beta V(h)$ as the total change of the grand potential when the colloidal sphere is brought from $h = \infty$ to a finite distance $h$:

$$\beta V(h) = \beta(\Omega_h - \Omega_\infty). \tag{7}$$

With the numerical solution of equations (2) inserted in equations (6) and (7), we have thus arrived at the effective interaction potential in full non-linear PB theory.

## 3. The interaction potential in linear theory

Due to the non-linearity of the PB equation, the BVP of equation (2) can in general only be solved numerically. Analytical work is feasible merely in the special case where $\phi$ is everywhere smaller than one, in which case linearization of the BVP of equation (2) becomes possible. But even then, as we will see soon, further approximation is needed to arrive at analytical expressions for the effective potential. Nevertheless, we begin by studying the

linear case, mainly for the reason that the basic features of our problem can best be understood at this level of approximation. In section 4, we then return to the non-linear theory formulated in equations (2) and (6).

Linearizing the PB equation in equation (2) leads to the following BVP:

$$\begin{aligned}
&\nabla^2\phi = \kappa^2\phi && \vec{r} \in G \\
&\nabla^2\phi = 0 && \vec{r} \in G_< \\
&\epsilon\vec{n}_w \nabla\phi\big|_{z=0+} - \epsilon'\vec{n}_w \nabla\phi\big|_{z=0-} = 4\pi\epsilon\lambda_B\sigma_w && \vec{r} \in \partial G_w \\
&\vec{n}_c \nabla\phi = 4\pi\lambda_B\sigma_c && \vec{r} \in \partial G_c \\
&\phi = 0 && \text{at } \infty.
\end{aligned} \tag{8}$$

The grand potential, too, becomes much simpler on linearization, because the volume integrals in equation (6) vanish due to the fact that $\phi \sinh\phi - 2(\cosh\phi - 1) \approx 0$ if $\phi < 1$. This leaves us with

$$\beta\Omega = -\frac{\sigma_w}{2}\int_{\partial G_w} \mathrm{d}S\ \phi - \frac{\sigma_c}{2}\int_{\partial G_c} \mathrm{d}S\ \phi - \beta W^{SE}. \tag{9}$$

We see that, in linear theory, the grand potential reduces to just the electrostatic energy of the system—that is, the electrostatic energy which the colloidal ($\sigma_c$) and interfacial charges ($\sigma_w$) have in the mean-field potential $\phi$. Carnie *et al* solved this BVP and calculated the effective colloid potential from it [22], which they later on compared with the numerical solution of the full PB equation [23]. Related studies on the double-layer interaction of two spheres in linearized theory can be found in [19, 24, 45].

### *3.1. The uncharged interface: image-charge and confinement effects*

The case of an uncharged interface ($\sigma_w = 0$) already reveals most of the physical content subsumed in the effective wall–colloid pair potentials. That there is a non-vanishing effective potential even in this case might at first seem surprising, but it becomes obvious if one realizes that the ionic double layer surrounding the colloid is heavily distorted from its usual bulk shape by the presence of the wall that is impenetrable to the ions. In addition to this confinement effect, we have to expect image-charge effects arising from the dielectric discontinuity across the interface. We now aim to discuss both effects by considering the case of a colloid near an uncharged wall.

Since the BVP of equation (8) still poses severe problems due to the complicated geometry of the region $G$, i.e., the shape of the boundaries $\partial G_c$ and $\partial G_w$, we simplify the problem a little further, and replace the colloidal sphere of finite size by a fixed *point-charge ion*—an approximation that is applicable when the particles are separated by distances much larger than their radii. For such a point charge, the linearized PB BVP of equation (8) takes the form

$$\begin{aligned}
&\nabla^2\phi = \kappa^2\phi + 4\pi\lambda_B Z\big[\delta(h-z)\delta(x)\delta(y)\big] && \vec{r} \in G \\
&\nabla^2\phi = 0 && \vec{r} \in G_< \\
&\epsilon\vec{n}_w \nabla\phi\big|_{z=0+} - \epsilon'\vec{n}_w \nabla\phi\big|_{z=0-} = 0 && \vec{r} \in \partial G_w \\
&\phi = 0 && \text{at } \infty
\end{aligned} \tag{10}$$

where we used the fact that $\sigma_c = Z/4\pi a^2$. This BVP has been solved by Stillinger [31], and independently by Schmutzer [32]. The Stillinger solution for the potential around a reference point ion of charge $-Ze$ at the position $h$ (see figure 1) reads

$$\phi_h^{St}(s,z) = -Z\lambda_B\kappa\int_0^\infty \mathrm{d}l\ J_0(\kappa s l)\frac{l}{\tilde{l}}\left(\mathrm{e}^{-\kappa|z-h|\tilde{l}} + \tilde{\chi}(l)\mathrm{e}^{-\kappa(z+h)\tilde{l}}\right) \tag{11}$$

where $s^2 = x^2 + y^2$ and $\tilde{l} = (1 + l^2)^{1/2}$. $J_0$ is the usual spherical Bessel function and the quantities $\tilde{\chi}(l)$ and $\chi$ are given by

$$\tilde{\chi}(l) = \frac{\epsilon\tilde{l} - \epsilon' l}{\epsilon\tilde{l} + \epsilon' l} = \frac{\alpha(\tilde{l} + l) - l}{\alpha(\tilde{l} - l) + l} \tag{12}$$

and

$$\chi = \frac{\epsilon - \epsilon'}{\epsilon + \epsilon'} = 2\alpha - 1 \tag{13}$$

where $\alpha = \epsilon/(\epsilon + \epsilon')$ gives a relation between the dielectric constants of the electrolytic solution and the substrate. The structure of the Stillinger potential can best be understood in the infinite-dilution limit $\kappa \to 0$, when equation (11) becomes [31]

$$\phi_h^0(s, z) = -Z\lambda_B \left[ \frac{1}{|\vec{r} - h\vec{e}_z|} + \frac{\chi}{|\vec{r} + h\vec{e}_z|} \right]. \tag{14}$$

In this limit, there is no screening by salt ions any more, and we are left with the purely electrostatic problem of a single point charge near a dielectric substrate, which is the classical test case for the image-charge method [33]. And, indeed, the second term of equation (14) can readily be identified as the potential due to the image charge at $z = -h$, while the first term is just the simple Coulomb potential of our original charge at $z = h$. This image charge has a magnitude of $\chi Ze$. It is easy to verify that $\phi^0$ of equation (14) does indeed solve the BVP of equation (10) in the limit $\kappa \to 0$, and satisfies, in particular, the complicated boundary condition at $\partial G_w$. The Stillinger potential in equation (11) for finite $\kappa$ has very much the same structure, with the first term, the direct term, coming from the (now screened) point ion and the second term, the indirect term, arising from the screened image charge. Consistently with this association, the first term becomes in the bulk limit (infinite colloid–wall distances) just the Yukawa potential of the standard Debye–Hückel (DH) theory, while the second vanishes.

In order to arrive at an effective potential, we next need to determine the grand potential as a function of $h$. Equation (9) in our case (uncharged wall, point ion) becomes

$$\beta\Omega_h = -\frac{Z}{2} \lim_{s\to 0, z\to h} \phi_h^{St}(s, z) - \beta W^{SE}. \tag{15}$$

The Coulomb self-energy $\beta W^{SE}$ of a point charge diverges, but so does the Stillinger potential in the limit $z \to h$, $s \to 0$, and their difference remains finite. Therefore, it is better to write

$$\beta\Omega_h = -\frac{Z}{2} \lim_{s\to 0, z\to h} \left[\phi_h^{St}(s, z) - \phi_h^C(s, z)\right] \tag{16}$$

where

$$\phi_h^C(s, z) = -Z\lambda_B \frac{1}{|\vec{r} - h\vec{e}_z|} = -Z\lambda_B\kappa \int_0^\infty J_0(\kappa s l) \mathrm{e}^{-\kappa|z-h|l} \, \mathrm{d}l \tag{17}$$

is just the direct Coulomb potential of the point charge, which we have rewritten using the identity [31]

$$\frac{1}{r} = \kappa \int_0^\infty J_0(\kappa s l) \mathrm{e}^{-\kappa z l} \, \mathrm{d}l. \tag{18}$$

Placing equation (17) and (11) into equation (16) and taking the limits, we obtain

$$\beta\Omega_h = \frac{Z^2\lambda_B\kappa}{2} \int_0^\infty \mathrm{d}l \left( \frac{l}{\tilde{l}} + \frac{l}{\tilde{l}} \tilde{\chi}(l) \mathrm{e}^{-2\kappa h\tilde{l}} - 1 \right) \tag{19}$$

which for $h \to \infty$ becomes

$$\beta\Omega_\infty = \frac{Z^2\lambda_B\kappa}{2} \int_0^\infty \mathrm{d}l \left( \frac{l}{\tilde{l}} - 1 \right) = -\frac{Z^2\lambda_B\kappa}{2}. \tag{20}$$

This latter energy looks familiar from the DH theory, where it is known as the DH self-energy, i.e., the interaction energy of a point test ion located in the bulk of a symmetric electrolyte and interacting with its ion atmosphere. With equations (19) and (20) we have finally arrived at the effective colloid–wall interaction potential:

$$\beta V_{SI}(h) = \beta(\Omega_h - \Omega_\infty) = \frac{Z^2\lambda_B\kappa}{2}\int_0^\infty \mathrm{d}l\ \frac{l}{\tilde{l}}\,\tilde{\chi}(l)\mathrm{e}^{-2\kappa h\tilde{l}}. \tag{21}$$

We notice that the integrand depends only on $\alpha = \epsilon/(\epsilon+\epsilon')$ and $\kappa h$; it can be evaluated only by numerical integration. But in the two most interesting limits, $\alpha \to 1$ and $\alpha \to 0$, equation (21) reduces to simple Yukawa-like energy expressions:

$$\beta V_{SI}(h) = \frac{Z^2\lambda_B\kappa}{2}\left(\frac{\mathrm{e}^{-2\kappa h}}{2\kappa h}\right) \qquad \text{if } \alpha = 1 \tag{22}$$

and

$$\beta V_{SI}(h) = -\frac{Z^2\lambda_B\kappa}{2}\left(\frac{\mathrm{e}^{-2\kappa h}}{2\kappa h}\right) \qquad \text{if } \alpha = 0. \tag{23}$$

$\alpha \to 1$ is the limit where the dielectric constant of the substrate, $\epsilon'$, is so much smaller than that of the solution (realized, for example, in the case of a glass/water or air/water interface) that $\epsilon'$ can be neglected against $\epsilon$; $\epsilon'/\epsilon \to 0$. The opposite limit, $\epsilon/\epsilon' \to 0$ ($\alpha \to 0$), describes the case where a substrate of extremely large dielectric constant is in contact with a solution of much smaller dielectric constant, e.g., a metal/water interface. In the limit of zero salt concentration ($\kappa \to 0$), we know from our discussion of equations (13) and (14) that in the two limits, $\alpha \to 1$ and $\alpha \to 0$, the point charge has image charges of the same magnitude. They differ, however, in their charge polarity, having the same polarity when $\alpha \to 1$ and just the opposite if $\alpha \to 0$. Thus, the point charge at position $h$ sees a potential $\pm Z\lambda_B/2h$ and the wall–colloid interaction potential is $\mp Z^2\lambda_B/4h$, which is negative if $\alpha \to 0$ and positive otherwise. A single point charge in water is therefore attracted to a metal surface, but repelled from an uncharged glass surface. Now, if there are salt ions present ($\kappa > 0$), this changes only inasmuch as the image charge is screened by the salt ions, which produces just the screening factor $\mathrm{e}^{-2\kappa h}$ in the potential, $\pm Z\lambda_B\mathrm{e}^{-2\kappa h}/2h$, and the interaction potentials then become the screened Yukawa potentials of equations (22) and (23). These effective potentials can therefore be understood as the interaction of the point charge with its own *screened* image charge, an interaction which is attractive if $\epsilon' \gg \epsilon$ and repulsive if $\epsilon' \ll \epsilon$. All other cases, $0 < \alpha < 1$, are covered by the effective potential of equation (21), which when plotted against the distance from the planar interface always lies between those of equations (22) and (23), as is evident from figure 2.

In figure 3 we show the effective potential of equation (21) when the point charge nearly touches the wall ($\kappa h = 0.8, 1.0, 1.2$), as a function of $\alpha$. This quantity may be interpreted as the energy gained or lost in bringing the point ion from infinity to the surface of the wall, and can be used to make predictions about the adsorption behaviour of colloids on dielectric walls. We see that adsorption is favoured if $\alpha \to 0$, while desorption is favoured for $\alpha \to 1$, as one would intuitively predict from our simple electrostatic considerations in the $\kappa \to 0$ limit. In his paper, Stillinger presents a similar curve (figure 2 of reference [31]) where the interaction energy $W$ of the point charge at $h = 0$ with its ion atmosphere is plotted as a function of $\alpha$. The far more important interaction between the point charge and its image has however been subtracted. This curve shows a monotonically *decreasing* behaviour, with $W$ changing its sign from + to − at $\alpha = 0.645$. From this figure, Stillinger predicts adsorption if $\alpha \to 1$ and desorption if $\alpha \to 0$. This is not correct; it is just the other way round, as we have seen, and the error is clearly due to the neglect of the direct interaction of the point charge with its

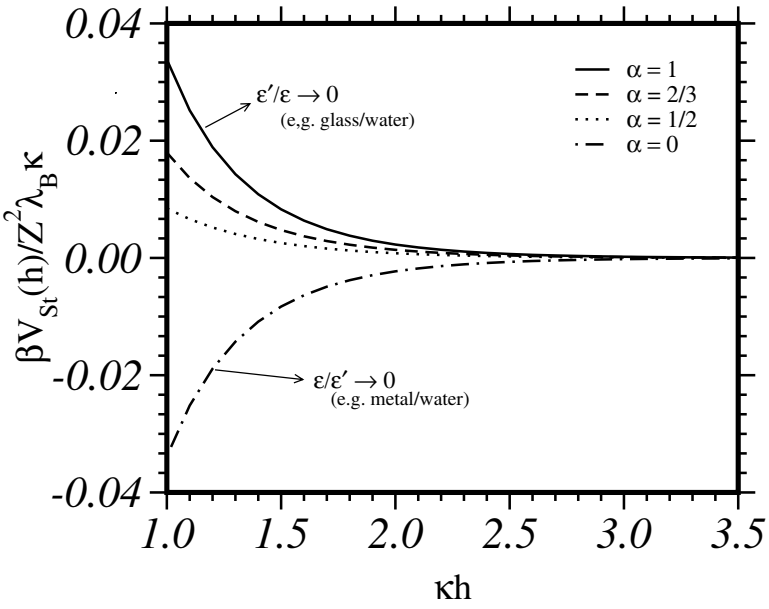


**Figure 2.** The effective colloid–wall interaction potential $\beta V_{St}(h)/Z^2\lambda_B\kappa$ for various values of $\alpha = \epsilon'/(\epsilon + \epsilon')$, calculated in linear theory. The macroion is considered as pointlike ($\kappa a = 0$).

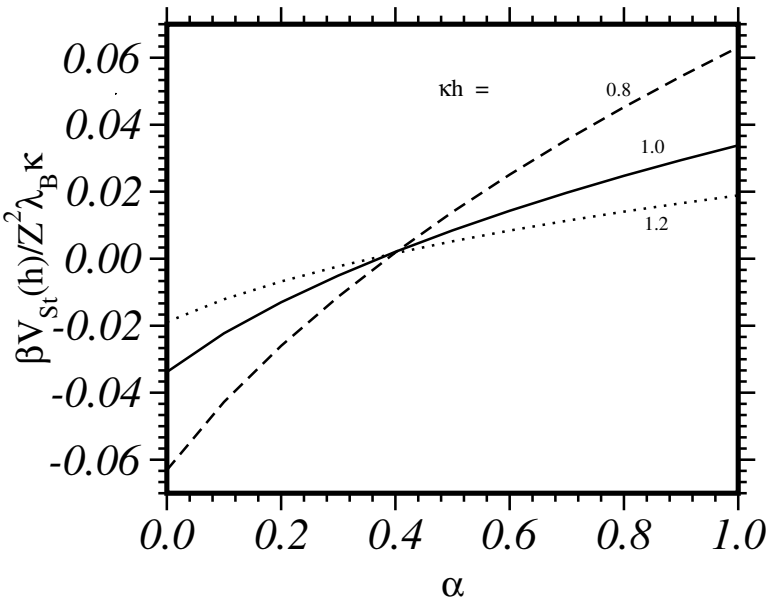


**Figure 3.** The effective potentials of figure 2 at fixed values of $\kappa h$, now as functions of $\alpha$.

image. The same error has been made by Earnshaw [11] who predicts an electrostatic trapping of colloids at an air/water interface due to an attractive colloid/wall interaction potential. The discussion given above clearly shows that a colloid in an aqueous suspension will be repelled from and not attracted to an air/water interface.

If the substrate has the same dielectric constant as the solution, $\epsilon = \epsilon'$ (i.e. $\alpha = 1/2$), there are no image charges, as we can see from equations (13) and (14). And still, the colloid is repelled from the wall; see figures 2 and 3. This is accounted for by the fact that the shape of the colloidal double layer deviates from its perfect spherical bulk shape when the colloid approaches the wall. This is so because of the presence of a wall which is, though having the same dielectric constant as the solution, still impenetrable to electrolyte ions. This distortion will necessarily cost free energy. Therefore, repulsion is to be expected, when the particle is sufficiently close to the wall for this effect to occur. We thus learn from figure 2 that the effective wall–colloid interaction is dominated by two effects: the confinement effect, on the one hand, and the image-charge effect, on the other, which both have a repulsive effect if $\alpha \geqslant 1/2$, and which compete with each other if $\alpha < 1/2$ (this means that a case is conceivable where the effective wall–colloid interaction is repulsive in spite of an attractive interaction between the charge and its image).

Both effects are usually present, though their relative importance for the effective potential is strongly dependent on $\alpha$. To discriminate between one effect and the other, one has to choose a substrate having the same dielectric constant as the solution, thus eliminating all image charges and leaving just the confinement effect.

The potential given in equation (11) is also well known in the theory of the electric double layer, where a simple electrolytic solution (without colloid!) near an interface is studied. The starting point of the so-called weak-coupling theory for the point-ion model of the double layer [35] is just the BVP of equation (10), with the important difference that the screening parameter $\kappa$ appearing in equation (10) itself depends on the density profile to be calculated [36]. This set of equations can only be solved iteratively, and to lowest order one finds just the Stillinger potential, equation (11)—see [36,37]—which gives the first, crude representation of ion–ion correlations in a double layer. Most of the discussion on image-charge and confinement effects is usually also in this context and can be found in good review articles on double-layer theory—for example in [35]; it is not new, nor are the potentials of equations (22) and (23), which appeared in the literature as early as 1924 in studies by Wagner [38] and Onsager and Samaras [39] on surface tension of electrolytes.

### *3.2. The uncharged interface: renormalizing the colloidal charge*

We now move on to correct the potential around the test point ion to take account of the finite size of a colloid. This follows from renormalizing the colloidal charge from $Z \to Z^* = Z/g$, a standard trick known from the theory of effective colloid/colloid interaction in bulk [28]. The primary error that is involved in representing the colloid by a point ion is that it allows microions to be in the region $r < a$ ($r$ is the distance from the centre of the colloid, $a$ its radius), where in reality they are excluded. If one determines the total charge (colloidal charge minus the total charge of salt ions) inside a virtual sphere of radius $a$, one obtains a charge $Z^{virt}$ which is only a fraction $g$ of the colloidal point charge $Z$, $Z^{virt} = gZ$. The renormalization trick now consists of the idea of taking a larger value $Z/g$ for the colloidal point charge, so that the total charge of all ions inside the sphere of radius $a$ becomes $Z^{virt} = gZ/g = Z$, i.e. the actual charge of the colloid. Then we can take this virtual sphere of effective charge $Z$ as representing our colloidal sphere of radius $a$. This should work well as long as the ion distribution around the point charge is essentially spherical, because the electric field outside a charged sphere contains no information about the field-producing distribution of ions inside the sphere; any spherically symmetrical distribution of the same total number of ions inside $a$ has the same field at $r > a$.

Let us start by considering the bulk situation ($h \to \infty$), where the electrostatic potential around our colloidal point charge reduces to the usual DH potential:

$$\phi(r) = -\frac{Z\lambda_B \mathrm{e}^{-\kappa r}}{r} \tag{24}$$

and the ion charge density becomes

$$\rho(r) = -2c_s\phi = \frac{Z\kappa^2 \mathrm{e}^{-\kappa r}}{4\pi r}. \tag{25}$$

The net charge inside the virtual sphere is hence

$$Z^{virt} = g_\infty Z = Z - 4\pi \int_0^a \rho(r) r^2 \, \mathrm{d}r \tag{26}$$

which leads us to the familiar result

$$g_\infty = \frac{1+\kappa a}{\mathrm{e}^{\kappa a}}. \tag{27}$$

Translating these ideas now to the situation where $h$ is finite, we have to carry out a two-dimensional integration to determine the net charge inside the virtual sphere, since the Stillinger potential depends on two variables, $s$ and $z$ (see equation (11)):

$$Z(1-g_h) = 2\pi \int_{h-a}^{h+a} \mathrm{d}z \int_0^{b(z)} s \, \mathrm{d}s \; \rho_h(s,z) \tag{28}$$

with $\rho_h(s,z) = -2c_s\phi_h^{St}(s,z)$ which is derived from the Stillinger potential and $b(z) = \sqrt{a^2-(z-h)^2}$. Using the integral identity

$$\int_0^\beta J_0[\alpha x] x \, \mathrm{d}x = \frac{\beta}{\alpha} J_1[\alpha\beta] \tag{29}$$

equation (28) can be reduced to

$$g_h = 1 - \int_0^\infty \mathrm{d}l \; \frac{I(l)}{\tilde{l}} (1 + \tilde{\chi}(l) \mathrm{e}^{-2\kappa h \tilde{l}}) \tag{30}$$

with

$$I(l) = 2 \int_0^A \mathrm{d}\xi \; (A^2 - \xi^2)^{1/2} J_1[l(A^2-\xi^2)^{1/2}] \mathrm{e}^{-\tilde{l}\xi} \tag{31}$$

where $\xi = \kappa(z-h)$ and $A = \kappa a$. For ease of evaluation, we take the limiting case $\tilde{\chi}(l) = 1$ ($\alpha \to 1$) in equation (30) and solve the resulting equation for $g_h$ by numerical integration. In figure 4, $g_h$ is shown for various values of $\kappa a$. It rises from the wall (interface) and approaches, as it should, the bulk limit $g_\infty$ as $\kappa h$ becomes large. The first value of each curve corresponds to a situation where $h = a$, i.e. where the particle touches the wall. Interestingly, this first value becomes first smaller with increasing $\kappa a$, up to $\kappa a = 1$, and goes up again for $\kappa a > 1$. This behaviour allows us to draw the conclusion that $g_h$ will never deviate by more than a few per cent from $g_\infty$, and it is thus not only a convenient, but also a very good, approximation to replace $g_h$ by the much simpler expression for $g_\infty$. This approximation we will henceforth adopt.

We can best summarize the results obtained so far by repeating the effective wall–colloid interaction potential for the case $\alpha = 1$. This is a case that is naturally of prominent interest in our context, since colloids in most experiments are suspended in aqueous solutions, and water has an extraordinarily large dielectric constant in comparison to practically every possible wall material, so making the assumption that $\epsilon'/\epsilon \to 0$ is almost always justifiable for colloidal

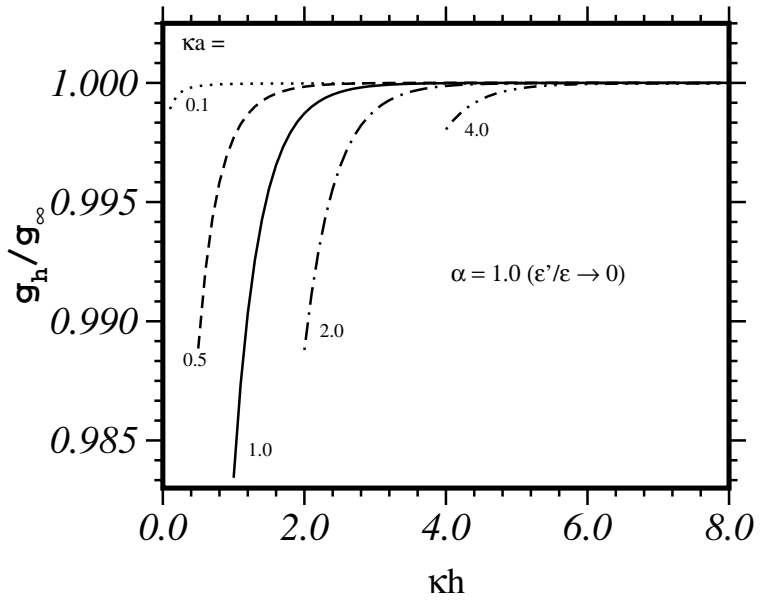


**Figure 4.** The ratio of the macroion renormalizing factor near the interface ($g_h$) to that of the bulk ($g_\infty$), versus the macroion–wall distance $\kappa h$, for $\alpha = 1$.

systems. In the following we shall therefore repeatedly focus on this important limiting case. Inserting $Z/g_\infty$ with $g_\infty$ from equation (27) into equation (22), we obtain the potential

$$\beta V_{St}(h) = \frac{Z^2 e^{2\kappa a}\lambda_B \kappa}{2(1+\kappa a)^2}\left(\frac{e^{-2\kappa h}}{2\kappa h}\right) \tag{32}$$

which demonstrates that increasing particle size results in increased repulsion from the wall. The potential in equation (32) is just half of the usual repulsive double-layer potential of DLVO theory between two like-charged spheres that are separated by a distance $2h$ from each other. This is clear: the BVP given in equation (8) reveals that the normal component of the electric field at the interface is zero in our case where $\epsilon'/\epsilon = 0$. This is exactly the same situation as on the mid-plane between two identical spheres. In other words, the electric field lines on the positive side of the symmetry plane are identical in the two cases (colloid/wall and colloid/colloid). The only difference is that in the colloid/colloid case the total volume filled by the electrolytic solution is just twice the volume in the colloid/wall case. Since the grand potential is obtained from the integration over this volume, this produces just a factor $1/2$, which then remains the only difference between equation (32) and the effective colloid/colloid interaction in the bulk.

### *3.3. The charged interface: the superposition principle*

After having considered the case where the surface charge density at the wall is zero ($\sigma_w = 0$), we now return to the starting point of this section, the BVP in linear theory, formulated in equation (8). The great advantage of linearization of the PB equation is that one can make use of the superposition principle; that is, if one knows the electrostatic potential $\phi$ for a single point charge, one can calculate the potential for an arbitrary charge distribution just by superposing the point-charge potentials. Therefore, we can reuse the Stillinger potential (which is just the

potential for a single point charge) as a Green's function for the more complex distribution of fixed charges appearing in the BVP of equation (8).

To be specific, let us assume that the single point charge, which in the Stillinger BVP of equation (10) has been located at $z = h$, is now at the position $(h_x, h_y, h_z)$. This point charge we now assume to have a charge $+e$. The Stillinger potential, given in equation (11), has to be modified then in the following obvious way:

$$\phi^{Gr}_{\vec{h}}(x, y, z) = \lambda_B \kappa \int_0^\infty \mathrm{d}l \; J_0(\kappa l[(x - h_x)^2 + (y - h_y)^2]^{1/2}) \frac{l}{\tilde{l}} (\mathrm{e}^{-\kappa|z-h_z|\tilde{l}} + \tilde{\chi}(l)\mathrm{e}^{-\kappa(z+h_z)\tilde{l}}). \tag{33}$$

This function is in fact the Green's function of our problem, equation (8); see [36,37]. Given an arbitrary distribution of fixed charges $\sigma(\vec{h})$, we can now generate the corresponding potential by convoluting $\sigma(\vec{h})$ with this Green's function:

$$\phi(x, y, z) = \int \phi^{Gr}_{\vec{h}}(x, y, z)\sigma(\vec{h}) \, \mathrm{d}\vec{h}. \tag{34}$$

For example, setting $\sigma(\vec{h}) = -Z\delta(h_x)\delta(h_y)\delta(h_z - h)$ and performing the integration in equation (34) leads us back to the original Stillinger potential, given in equation (11). For the homogeneously charged interface at $z = 0$, we demand $\sigma(\vec{h}) = -\sigma_w\delta(h_z)$, which when inserted in equation (34) gives a potential

$$\phi^{\sigma_w}(x, y, z) = -4\pi \frac{\sigma_w \lambda_B}{\kappa} \mathrm{e}^{-\kappa z} \tag{35}$$

that can easily be verified to be a solution to the BVP of equation (8) when there is no colloid. We note, in passing, that equation (35) is independent of $\epsilon'$, which is reasonable since the electric field at $z < 0$ is zero and the dielectric property of the wall material thus irrelevant. The general solution to the BVP in equation (8) may be obtained from convoluting

$$\sigma(\vec{h}) = -\sigma_w\delta(h_z) - \sigma_c\delta(\sqrt{h_x^2 + h_y^2 + (h_z - h)^2} - a) \tag{36}$$

with the Green's function, equation (33)[1]. Since this is a rather involved undertaking [19,22] leading again to non-analytical expressions, we must once more be content with the point-charge assumption for the colloid:

$$\sigma(\vec{h}) = -\sigma_w\delta(h_z) - Z\delta(h_x)\delta(h_y)\delta(h_z - h) \tag{37}$$

resulting in a potential which is nothing but the sum of the potentials of equations (11) and (35), $\phi^{St}_h$ and $\phi^{\sigma_w}$.

To obtain the effective potential, we need to look back at equations (7) and (9) which lead us to

$$\beta V(h) = \beta V_{St}(h) - \frac{\sigma_w}{2} \int_{\partial G_w} \mathrm{d}S \; \phi^{St}_h - \frac{Z}{2}\phi^{\sigma_w}(h) \tag{38}$$

where the first term is the effective potential in the case of an uncharged wall, given in equation (21), while the second and third terms give the interaction of the interfacial charges with the field produced by the colloidal point charge and vice versa. These two latter terms are equal, so

$$\beta V(h) = \beta V_{St}(h) - Z\phi^{\sigma_w}(h) \tag{39}$$

[1] This is not quite correct, since we assumed a vanishing dielectric constant inside the colloidal sphere in our boundary value problem of equation (8), while a superposition of potentials of point charges fixed at the surface of the colloids implies that the dielectric constant inside the sphere is the same as that outside.

which for $\alpha = 1$ ($\epsilon'/\epsilon \to 0$) takes the form

$$\beta V(h) = \frac{Z^2 \lambda_B \kappa}{2} \left( \frac{e^{-2\kappa h}}{2\kappa h} \right) + Z\, 4\pi \frac{\sigma_w \lambda_B}{\kappa} e^{-\kappa h}. \tag{40}$$

From this expression it is evident that the colloidal point charge interacts with two well-separated charge distributions at the same time: with the interfacial charges, on the one hand, and the image charge, on the other. Both are screened, but one of them is a distance $h$ away, and the other $2h$. The second term ($\sim e^{-\kappa h}$), describing the direct interaction of the point charge interacting with the unperturbed double layer of the charged wall, will therefore be the dominant one for larger distances. The image-charge term, though having a pre-factor that goes as $Z^2$, becomes important only for small distances and small surface charge densities $\sigma_w$. We expand on this further, below. Again, renormalization of the colloidal charge is useful:

$$\beta V_{LIN}(h) = \frac{Z^2 \lambda_B \kappa}{2(1+\kappa a)^2} \left( \frac{e^{-2\kappa(h-a)}}{2\kappa h} \right) + Z\, 4\pi \frac{\sigma_w \lambda_B}{\kappa(1+\kappa a)} e^{-\kappa(h-a)}. \tag{41}$$

Netz, in a recent paper, derived the Green's function of equation (33) within a field-theoretic formalism [34]. He considered the more general case, where there are mobile ions *within* the interface itself (salty interface) and two solutions with different salt concentrations and dielectric constants on either side of the interface. We here just want to mention the effect produced by the salty interface. Such a two-dimensional salt solution is realized, for instance, by membranes consisting of cationic and anionic lipids [6].

To allow for a salty interface, the only thing to be changed is the function $\tilde{\chi}$ in equation (12); the rest of the Green's function in equation (33) remains the same; see reference [34]. If $\kappa_=$ is the screening constant of the 2D interfacial salt, the function $\tilde{\chi}$ now becomes

$$\tilde{\chi}_=(l) = \left( \epsilon \tilde{l} - \epsilon' l - \frac{\kappa_=}{\kappa} \epsilon \right) \Big/ \left( \epsilon \tilde{l} + \epsilon' l + \frac{\kappa_=}{\kappa} \epsilon \right). \tag{42}$$

Approximating the colloid again by a point charge, we can repeat the scheme outlined in the previous sections, and will again arrive at the effective potential of equation (21), except that $\tilde{\chi}$ is now to be replaced by $\tilde{\chi_=}$. The integration over the variable $l$ can again be performed only in certain limiting cases. For $\alpha = 1$, one finds the effective potential

$$\beta V_=(h) = \frac{Z^2 \lambda_B \kappa}{2} \left( \frac{e^{-2\kappa h}}{2\kappa h} \right) \left( 1 - \frac{2\kappa_=}{\kappa_= + \kappa} \right) \tag{43}$$

which is to be compared with equation (22) of the Stillinger case. If, in addition, one wants to allow for interfacial charges, one obtains an effective potential as in equation (40), with $\beta V_=(h)$ of equation (43) replacing the first term. We see that the repulsive Stillinger effective potential now competes with an attractive potential that arises from the mobile ions in the interface. These ions show a strongly inhomogeneous distribution centred at the point ($x = 0$, $y = 0$) on the interface, in order to optimize the screening of the point charge. Though the interface on average is still neutral, this accumulation of ions at ($x = 0$, $y = 0$) leads to additional electrostatic attraction between the wall and the colloid. Equation (43) states that beyond a certain concentration of ions in the interface ($\kappa_= > \kappa$) this can actually result in an attractive wall–colloid interaction. Thus, the repulsive effect of image charges tends to be less pronounced if there are mobile screening ions in the interface, but the distance dependences ($\sim e^{-2\kappa h}/2\kappa h$) of the two effects are the same.

## 4. The interaction potential in non-linear theory

The BVP that we actually set out to study is that of equation (2). Due to its non-linear nature it cannot be solved analytically (see however reference [24]). It is therefore impossible to give

an analytical expression for the effective wall–colloid potential which is valid in a parameter regime where the non-linearity becomes important. On the other hand, the condition $\phi < 1$ for linearization is rather restrictive, and most experiments are carried out in a parameter regime where this condition is not fulfilled. One way out of this problem is to make use of the effective-charge concept, used already in the last section to take account of the finite size of the colloid. Reusing the outer form of the potential obtained in linear theory, one can renormalize the charge yet again, for the purpose of including—on a rather phenomenological level—non-linear effects [28]. Another way to go beyond linear theory is to use the few known solutions to non-linear problems in other geometries (for example, planar wall) in order to improve on the potentials calculated in linear theory. That is what we want to do now, starting from equation (40), which is valid for the case $\alpha \to 1$ (this case is the only one that we consider in this section). Since we can calculate the full numerical solution of equation (2) and with it the effective potential in non-linear theory, equation (6), we can test in what parameter regime and to what extent these augmented potentials work.

The PB equation for the sphere/plate geometry has been solved by others before [23,25,26]. The work of Stankovich and Carnie [23] can be regarded as the extension of a previous study by these authors on double-layer forces between similar spheres [21]. In this paper the validity of classical theories of effective colloidal pair potentials is checked against accurate numerical results, as has been done in a similar way in [40]. Earlier numerical studies of the PB equation for two spheres can be found in [41,42], where approximate interaction potentials [43] have been checked, but Carnie *et al* in [21] were the first to really make detailed quantitative statements regarding the ranges of validity of different approximations.

### *4.1. Approximate potentials and their regimes of validity*

The BVP of equation (2) can be solved if there is no colloid but just a planar charged wall, and the solution (Gouy–Chapman solution [44]) is

$$\phi^{GC}(z) = 4\,\mathrm{arctanh}(\mathrm{e}^{-\kappa z}\tanh(\Phi_w/4)) \tag{44}$$

with $\Phi_w$ being the potential at the wall. The derivative of this potential with respect to $z$ at $z = 0$ is $-2\kappa \sinh \Phi_w/2$, which according to equation (2) must be equal to $4\pi\lambda_B\sigma_w$. This gives the Graham equation [9,44] relating the surface charge densities to the surface potentials:

$$4\pi\lambda_B\sigma_{w/c} = -2\kappa \sinh \Phi_{w/c}/2. \tag{45}$$

For later usage, we have already introduced the subscript $c$ referring to the colloidal charge densities and surface potentials. Using equation (45), we introduce another abbreviation:

$$\gamma_{w/c} = |\tanh \Phi_{w/c}/4| = \tanh\left[\frac{1}{2}\,\mathrm{arcsinh}\left(\frac{2\pi\lambda_B\sigma_{w/c}}{\kappa}\right)\right]. \tag{46}$$

If $\kappa z > 1$, equation (44) becomes

$$\phi^{GC}(z) = -4\gamma_w \mathrm{e}^{-\kappa z} \tag{47}$$

because $\gamma_w$ cannot be larger than one. Note that if $\Phi_w < 1$, equation (47) reduces to equation (35).

The second term in the interaction potential obtained in linear theory, equation (40), is just the electrostatic energy of a point charge $Z$ in the unperturbed double layer of the charged wall. We can go beyond linear theory and improve this interaction potential just by taking $\phi^{GC}(z)$ of equation (47) instead of $\phi^{\sigma_w}(z)$, equation (35), in expression (39). This, along with the usual renormalization of charge $Z/g_\infty$ ($g_\infty$ from equation (27)), leads to the potential

$$\beta V_{GCH}(h) = \frac{Z^2\lambda_B}{2(1+\kappa a)^2}\left(\frac{\mathrm{e}^{-2\kappa(h-a)}}{2h}\right) + \frac{Z4\gamma_w}{1+\kappa a}\mathrm{e}^{-\kappa(h-a)} \tag{48}$$

which henceforth we call the Gouy–Chapman-based (GCH-based) potential. If the surface potential of the wall becomes small, $\beta V_{GCH}(h)$ reduces to $\beta V_{LIN}(h)$ of linear theory, equation (41), because $\phi^{GC}(z)$ reduces to $\phi^{\sigma_w}(z)$.

If $\kappa a > 1$, we can use equation (47) yet again to represent also the double layer surrounding the colloidal particle. Formally, this can be done by renormalizing the charge anew. Starting with equation (24) with $Z$ replaced by $Z^*/g_\infty$ and requiring $\phi(a)$ to be just $\phi^{GC}(0)$ of equation (47), one finds $Z^* = 4\gamma_c(1+\kappa a)a/\lambda_B$; see reference [28]. Using this $Z^*$ instead of $Z$ in equation (48), one obtains

$$\beta V_{DJG}(h) = \frac{4\gamma_c^2 a}{\lambda_B} e^{-2\kappa(h-a)} + \frac{16a\gamma_c\gamma_w}{\lambda_B} e^{-\kappa(h-a)}. \tag{49}$$

The conventional way to derive equation (49) is to calculate the free energy of an electrolytic solution in between two parallel plates having surface charge densities $\sigma_w$ and $\sigma_c$ and then to integrate over these energies to account for the curvature of the colloidal sphere (the Derjaguin approximation [9,27]). However, we emphasize that this derivation gives only the second term in equation (49), while ours leads also to the image-charge interaction terms. In the following, we will refer to the potential of equation (49) as the Derjaguin-based (DJG-based) potential.

The derivation of the potentials in equations (48) and (49) might appear rather *ad hoc*, and it is therefore an advantage that we can calculate correct mean-field interaction potentials to test the validity of $V_{GCH}(h)$ and $V_{DJG}(h)$. The most prominent deficiency of these two potentials is an obvious inconsistency: in just adding the image charge to the direct interaction one has still relied on the superposition principle that is strictly valid only in linear theory, while introducing at the same time the double-layer potential of the non-linear Gouy–Chapman theory. One should therefore expect a good agreement with the potentials derived from PB theory only if the non-linearity is weak. In the highly non-linear regime, this inconsistency is almost bound to produce a substantial error, and, as we will see, the case can occur where it is even better to ignore the image-charge contribution than to include it in this inconsistent way.

We have now introduced four interaction potentials based on approximations that are valid in different parameter regimes. These are $V_{GCH}(h)$ of equation (48), $V_{DJG}(h)$ of equation (49), $V_{LIN}(h)$ of equation (41), and, included in the latter, the Stillinger potential $V_{St}(h)$ for the neutral wall, equation (32). By comparing each of them with the exact PB solution obtained from equations (2) and (6) (see the appendices), we now want to find out for what regions of parameters these potentials are reasonably good approximations to the correct mean-field potential. There are again four parameters on which the four potentials depend, two specifying the surface charge densities of the wall and the colloid, and two for the size of the colloid and its distance to the wall, both in units of $1/\kappa$. While the latter two parameters are therefore just $\kappa a$ and $\kappa h$, the first two are best expressed in terms of surface potentials, $\Phi_c$ and $\Phi_w$, which can be obtained from equation (45) for any given pair of surface densities. The parameters $\Phi_c$ and $\Phi_w$ are only used here for convenience and are not intended to imply anything about the boundary conditions; we reiterate that we used constant-charge boundary conditions in all of our calculations. For equation (48), we need a value for $Z\lambda_B\kappa$, which is also specified by $\Phi_c$ using $\sigma_c = Z/4\pi a^2$, $Z\lambda_B\kappa = 2(\kappa a)^2|\sinh\Phi_c/2|$. To quantify the accuracy of the potentials under investigation, we define the relative percentage error

$$\%\ \text{Error} = \left(\frac{\text{analytical} - \text{numerical}}{\text{numerical}}\right) \times 100\%. \tag{50}$$

This equation will reveal where the approximate theories overestimate (positive values) the interaction and where they are underestimated (negative values). Results are presented for various $\Phi_w$:$\Phi_c$ ratios up to 4:4, for particle radius $\kappa a$ from 1 to 10 and minimum wall–particle distance $\kappa(h-a)$ up to 5.

*The Stillinger potential, $V_{St}(h)$.* We begin the presentation of our results again with the case of an uncharged wall and concentrate on $V_{St}(h)$ of equation (32) (which is identical to $V_{GCH}(h)$ and $V_{LIN}(h)$ when $\Phi_w = 0$). In figure 5(a), we compare this potential with the PB-based potential for $\Phi_c = 1.0, 1.5, 2.0$ taking a fixed value for $\kappa a$ of 5.0. Evidently, the Stillinger potential tends to systematically overestimate the correct potential. To quantify this error, we used the curves of figure 5(a) and calculated from equation (50) the percentage error for all three values of $\Phi_c$; the results are shown in figure 5(b). For $\Phi_c = 1.0$ the agreement between the PB-based potential and $V_{St}(h)$ is better than 10% for nearly all wall–colloid distances ($\kappa(h - a) > 0.6$). Recalling that $\Phi = 1$ marks the value where the non-linearity becomes important, this is what one would have expected for the Stillinger potential, since it is derived in the linear approximation. For larger values of $\Phi_c$, going up in the weakly non-linear regime only, we see that the Stillinger potential soon becomes rather poor, with a percentage error as high as 30% at all wall–colloid distances for a value of only $\Phi_c = 2.0$.

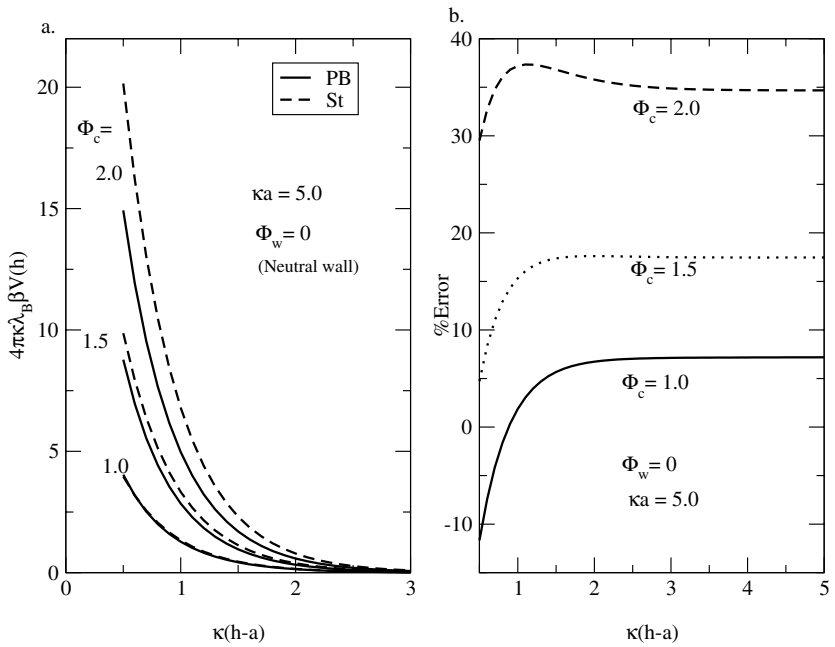


**Figure 5.** Uncharged wall, $\kappa a$ fixed: comparison of the effective wall–colloid potentials based on (i) an approximate potential, equation (32), and (ii) the solution to the full PB equation (constant-charge boundary conditions). Different values of the reduced surface potential $\Phi_c$ of the colloid are considered. (a) The interaction potential, $4\pi\lambda_B\kappa\beta V_{St}(h)$, versus the wall–colloid minimum separation, $\kappa(h - a)$. (b) The accuracy of the effective potentials in (a), percentage error versus $\kappa(h - a)$.

So far we have just considered the case $\kappa a = 5$. To get a more systematic overview of the accuracy of $V_{St}(h)$, in particular for different combinations of $\kappa a$ and $\kappa h$, we now introduce a different form of presentation of our data, used first by Glendinning and Russel [45] and later extensively by Carnie *et al* [19,21]. It is that of indicating in the parameter space $(\kappa a, \kappa h)$ those regions where the percentage error is less than 10%. In figure 6, we have plotted these lines of 10% error for the Stillinger case, for the three values of $\Phi_c$ already used in the previous figure ($\Phi_c = 1.0, 1.5, 2.0$). Each line in this plot separates a region in the $(\kappa a, \kappa h)$ space where the error of $V_{St}(h)$ is less than 10% from a region where it is greater the 10%. In this plot and

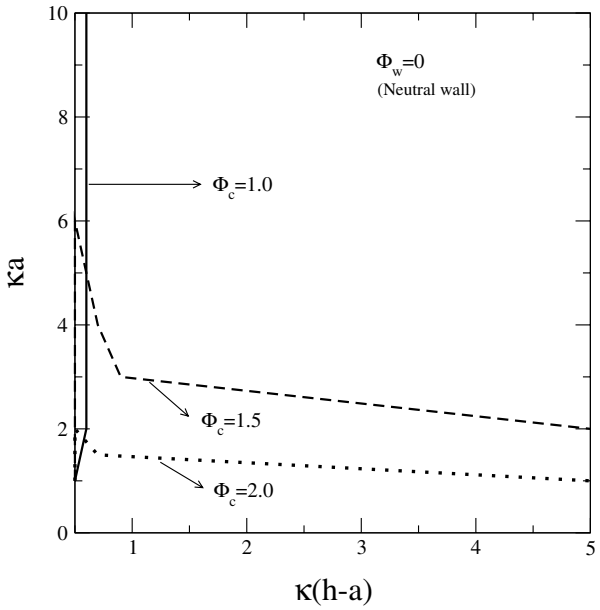


**Figure 6.** Uncharged wall, $\kappa a$ varies: regions in the $(\kappa a, \kappa h)$ plane where the error of the approximate potential, equation (32), is below 10%. Arrows point to the regions with under 10% error. The values of $\Phi_c$ are the same as in figure 5.

all those of this type that follow, the arrows always point into the region where the error is *below* 10% and thus where the potential investigated is a reasonably good approximation to the PB-based potential. Since the Stillinger potential $V_{St}(h)$ depends merely on three parameters ($\kappa a$, $\kappa h$, and $\Phi_c$ since $\Phi_w = 0$), figure 6 contains information on the error of $V_{St}(h)$ for *all possible* combinations of parameters.

We produce such contour diagrams from error curves like those of figure 5(b). For example, the error curve for $\Phi_c = 1.0$ in figure 5(b) is between $-10\%$ and $+10\%$ for $\kappa(h-a) > 0.6$, which is consistent with the solid line of figure 6 going through the point $(\kappa a, \kappa(h-a)) = (5.0, 0.6)$ and with the arrow on the solid line pointing into the region where $\kappa(h-a) > 0.6$. Figure 6 shows clearly that the Stillinger potential, equation (32), produces an error smaller than 10% for almost all values of $\kappa a$ as long as $\Phi_c \leqslant 1$ and $\kappa(h-a) > 0.6$. Thus we can make the general statement that the Stillinger potential is within 10% error over the whole linear regime ($\Phi_c \leqslant 1$) just as long as $\kappa(h-a) > 0.6$. For larger values of $\Phi_c$, this potential soon fails, as we have already noticed in figure 5. For a moderately high value of the surface potential of only $\Phi_c = 2.0$, $V_{st}(h)$ has an error below 10% only if $\kappa a$ is rather small ($\kappa a < 1$)—see the dotted line in figure 6—and this is true for all colloid–wall distances. For even higher values of $\Phi_c$, the region of validity of the Stillinger potential in the $(\kappa a, \kappa h)$ plane will become even smaller, and at $\Phi_c = 3.0$ there is no point left in the $(\kappa a, \kappa h)$ plane where $V_{st}(h)$ has an error below 10%.

*The linear potential $V_{LIN}(h)$ and the GCH potential $V_{GCH}(h)$.* Let us now turn to the case where the wall bears interfacial charges ($\sigma_w > 0$). Figure 7(a) compares the linear and the GCH interaction potentials with the PB-based potential, again for $\kappa a = 5.0$ and $\Phi_c = 1.0$ and $\Phi_c = 2.0$ as in figure 5(a), but now with a surface wall potential of $\Phi_w = 1.0$. Again, the analytic potentials overestimate the correct potential for larger values of $\Phi_c$, which shows more clearly in figure 7(b), where the curves of figure 7(a) have been used to calculate the percentage

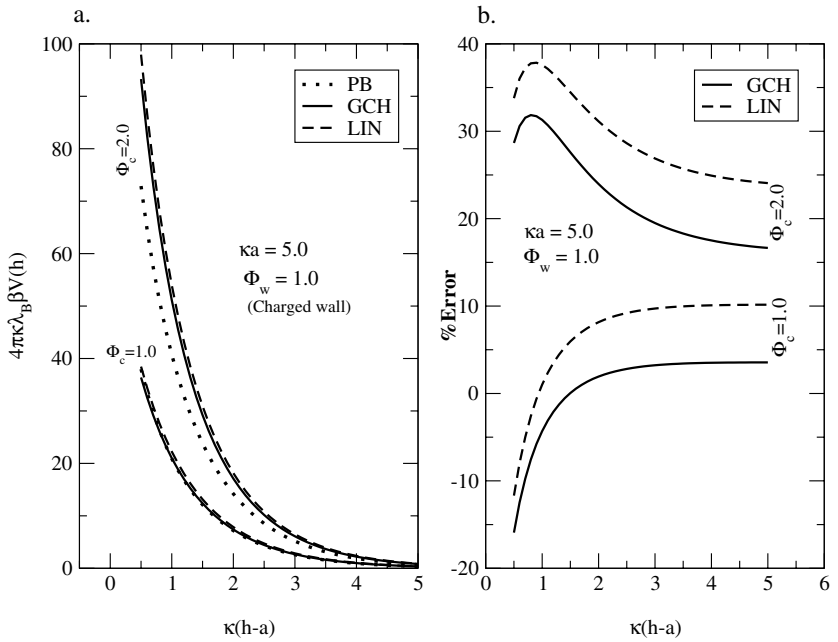


**Figure 7.** Charged wall, $\kappa a$ fixed: comparison of the effective wall–colloid interaction potentials based on (i) the linear potential (LIN), equation (41), (ii) the approximate potential (GCH), equation (48), and (iii) the full numerical solution of the PB equation. For a fixed wall–surface potential $\Phi_w = 1.0$, the colloid surface potential is varied from $\Phi_c = 1.0$ to $\Phi_c = 2.0$. (a) The interaction potential, $4\pi\lambda_B\kappa\beta V(h)$, versus the wall–colloid minimum separation, $\kappa(h-a)$. (b) The accuracy of the effective potentials in (a), percentage error versus $\kappa(h-a)$.

error according to equation (50). Again, for $\Phi_c = 1$, both potentials $V_{LIN}(h)$ and $V_{GCH}(h)$ show error less than 10% for almost all values of $\kappa(h-a)$, while the error for $\Phi_c = 2.0$ can reach values between 30% and 40%. Because the Stillinger potential is part of $V_{LIN}(h)$ and $V_{GCH}(h)$, this is what one would have anticipated from the failure of the Stillinger potential in this weakly non-linear regime found in figure 5(b). Figure 7(b) also demonstrates that $V_{GCH}(h)$ always has a smaller error than $V_{LIN}(h)$, a statement whose validity we have tested for a large number of input parameters. As $V_{LIN}(h)$ is merely a limiting case of $V_{GCH}(h)$ in the limit of small surface wall potentials, this is not surprising; it is still reassuring to know that the replacement of equation (35) by $\phi^{GC}(z)$ of equation (47) in the derivation of $V_{GCH}(h)$ does indeed mean an improvement of the potential. As $V_{LIN}(h)$ is thus contained in $V_{GCH}(h)$, we do not need to consider it any further and can instead concentrate on $V_{GCH}(h)$.

An overview can again be obtained from a contour plot in the $(\kappa a, \kappa h)$ parameter plane, figure 8, showing regions where the error is less than 10%. We have generated this contour plot by analysing error curves like those given in figure 7(b). We tested eight different combinations of $\Phi_w$ and $\Phi_c$, fixing the colloid surface potential at $\Phi_c = 1.0$ and varying $\Phi_w$ between one and four in figure 8(a), while fixing the wall potential and varying the colloid surface potential in figure 8(b). The two figures together now help us to identify the region of the four-dimensional parameter space where the GCH potential is a reliable and useful effective potential:

(i) As long as $\Phi_c \leqslant 1$ and $\kappa(h-a)$ is well above one, $V_{GCH}(h)$ is almost always a suitable potential, working well even for very large surface–wall potentials and showing only a very weak dependence on the colloidal size. That is what one can learn from figure 8(a).

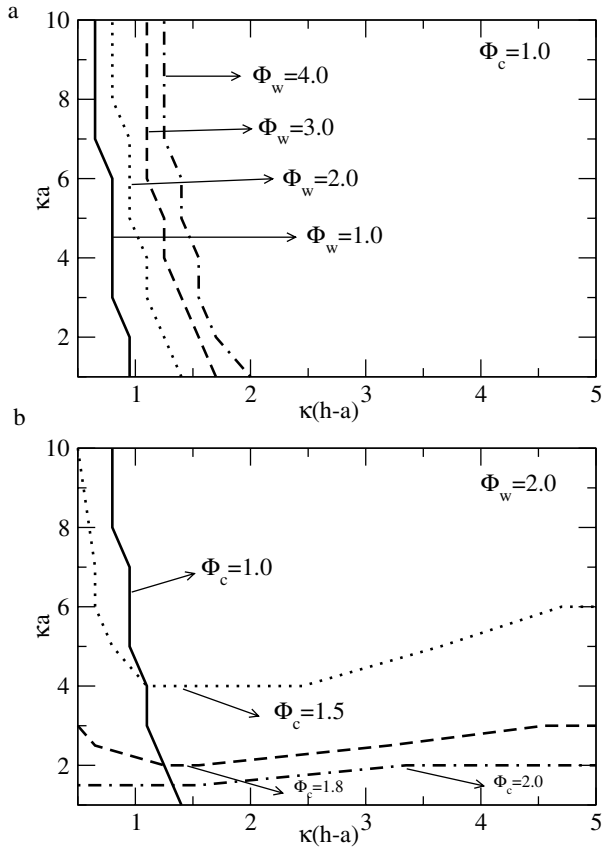


**Figure 8.** Charged wall, $\kappa a$ varies: an error contour diagram as in figure 6, but now for the GCH potential, equation (48). The arrows point to the regions with under 10% error.

(ii) If the colloid surface potential $\Phi_c$ is increased (figure 8(b)), the performance of $V_{GCH}(h)$ becomes poorer, and the region in the $(\kappa a, \kappa h)$ plane where $V_{GCH}(h)$ has a small error shrinks. For example, if $\Phi_w{:}\Phi_c \equiv 2{:}2$, $V_{GCH}(h)$ is useful only if $\kappa a$ is small ($\kappa a < 2$) (dashed–dotted line figure 8(b)).

We pointed out earlier that both non-linear potentials, equation (48) and equation (49), suffer from the same basic problem. In linear theory, the total electrostatic potential around interacting charged objects in an electrolytic solution can be obtained just by adding the separate potentials for each object in isolation, and as a result of this superposition principle the effective interaction between the objects is a simple sum of terms associable with the different charge distributions. This is not valid in non-linear theory, and still both potentials, equation (48) and equation (49), are obviously based on this principle as they are sums of direct and image-charge interactions. One might wonder whether this inconsistency is responsible for the bad performance of $V_{GCH}(h)$ at high $\Phi_c$, and whether or not the inclusion of the image-charge effect in equation (48) improves the effective potential at all. Figure 9 clarifies this point. We plotted the percentage error of $V_{GCH}(h)$ for $\Phi_w{:}\Phi_c \equiv 1{:}1$ and $\Phi_w{:}\Phi_c \equiv 2{:}2$, with (solid line) and without (dashed line) the first term in equation (48). We first observe that both lines in both cases converge for larger values of $\kappa h$; then the distance is too large for the image charge to have any effect at all (the image-charge interaction goes as $e^{-2\kappa(h-a)}$ and the direct interaction

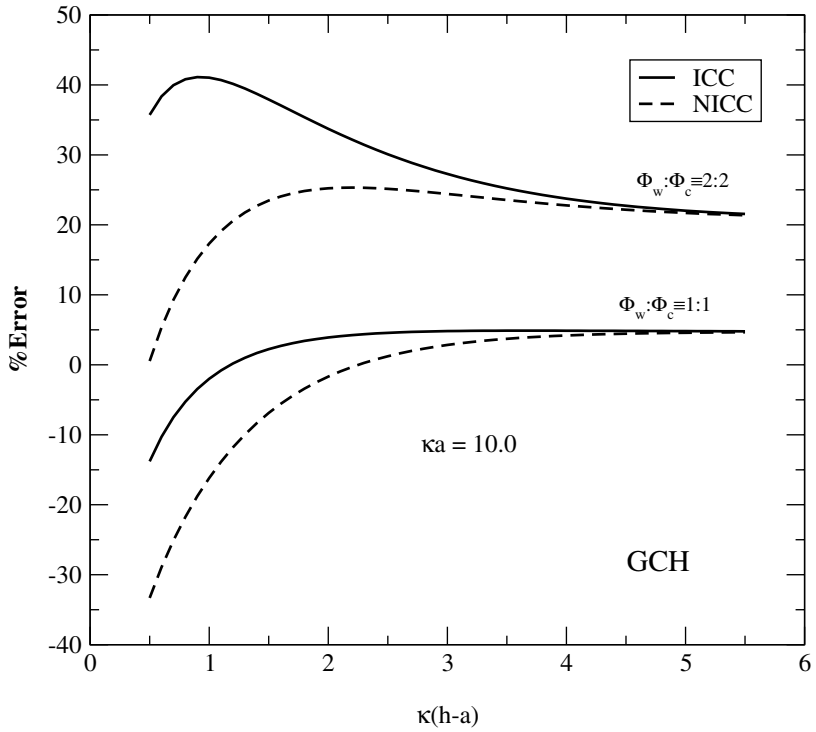


**Figure 9.** The contribution of image-charge term to the GCH potential, equation (48), for two combinations of $\Phi_w$:$\Phi_c$, $\kappa a = 10.0$: the full lines show the error of the GCH potential calculated with image-charge contributions (ICC), while the dashed lines show the error calculated with no image-charge contributions (NICC).

as $e^{-\kappa(h-a)}$). We furthermore observe that for $\Phi_w$:$\Phi_c \equiv$ 1:1 inclusion of the image-charge contribution considerably *improves* the accuracy of the potential, in particular in the range $1 < \kappa(h-a) < 3$. The case $\Phi_w$:$\Phi_c \equiv$ 2:2, on the other hand, shows that adding the image-charge term can also increase the error, thus demonstrating that the direct and the image-charge interactions are not additive in the non-linear regime. But we also note that the error is still quite large even if the image-charge effect is ignored.

Since it is the aim of this study not only to test approximate theories, but also to recommend for any given set of parameters ($\kappa a$, $\kappa h$, $\Phi_w$, $\Phi_c$) a handy analytical expression that is as close as possible to the mean-field result, we have to check whether one may substantially enlarge the total region with an error below 10% in figure 8 by totally ignoring the image-charge effect. The answer is negative. For the specific combinations of parameters which we found $V_{GCH}(h)$ to be a suitable potential for, we have explicitly tested that inclusion of the image-charge effect does indeed improve the agreement with the PB-based potential. This is not so for $V_{DJG}(h)$, which we discuss now.

*The DJG potential* $V_{DJG}(h)$. Like in figure 9, we check in figure 10 the importance of the image-charge interaction term, but now in the DJG potential $V_{DJG}(h)$. The same parameters as in figure 9 are used. Again, including the image-charge effect improves the result for $\Phi_w$:$\Phi_c \equiv$ 1:1, but causes a larger error for $\Phi_w$:$\Phi_c \equiv$ 2:2. In contrast to $V_{GCH}(h)$ in figure 9, $V_{DJG}(h)$ becomes better at larger distances when going from $\Phi_w$:$\Phi_c \equiv$ 1:1 to $\Phi_w$:$\Phi_c \equiv$ 2:2. One recognizes that for $\Phi_w$:$\Phi_c \equiv$ 2:2 the error without the image-charge

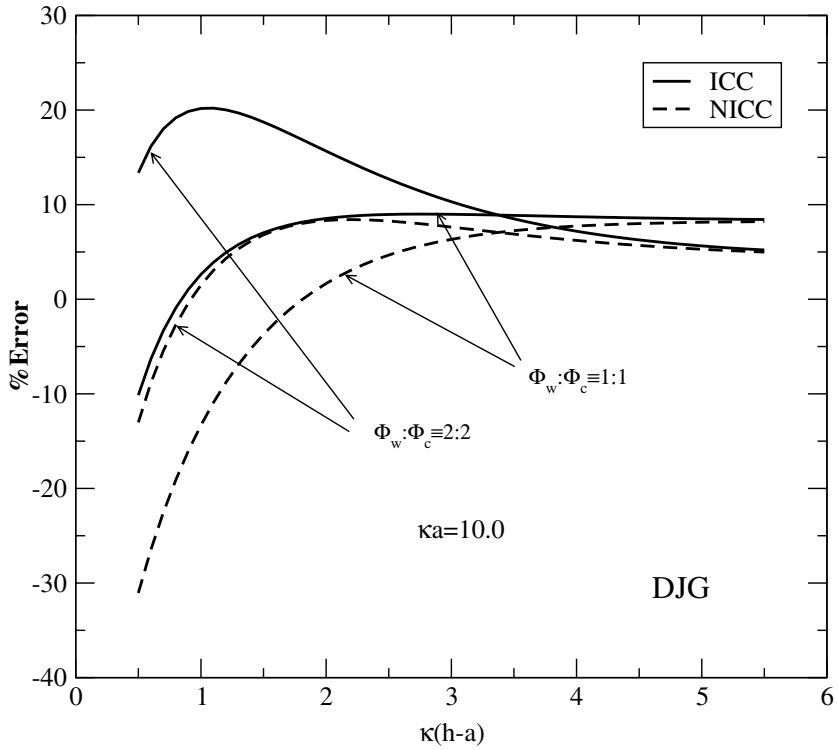


**Figure 10.** The contribution of the image-charge term to the DJG potential, equation (49). The parameters are the same as in figure 9. The full lines show the error of the DJG potential calculated with image-charge contributions (ICC), while the dashed lines show that with no image-charge contributions (NICC).

contribution remains well under 10%, while it goes up to 20% if the image-charge term is taken into account. This shows that naively adding the image-charge contribution can render a potential useless that would otherwise reproduce the mean-field result well (error $< 10\%$). We have checked this more systematically by producing 10% error contour maps as in figure 8 for the DJG potential with and without the image-charge contribution. We have found that for low values of $\Phi_c$ and/or low values of $\kappa a$, the first term in equation (49) is important. However, comparing the errors of $V_{DJG}(h)$ and $V_{GCH}(h)$ in this regime we have found that $V_{GCH}(h)$ generally produces a smaller error and is thus preferable to $V_{DJG}(h)$. On the other hand, in the parameter region where $V_{DJG}(h)$ performs better than $V_{GCH}(h)$, inclusion of the image-charge effect may considerably increase the error of $V_{DJG}(h)$, as seen for example in figure 10 for $\Phi_w$:$\Phi_c \equiv$ 2:2. The conclusion to be drawn from this is that adding direct and image-charge interactions as is done in equation (49) introduces an error that can sometimes be larger than the error that one produces by completely ignoring image charges. Of course, this conclusion is not meant to deny the existence of image charges, nor is it to say that they are unimportant; it just refers to the quality and usefulness of certain approximations. Moreover, it is true only in some region of parameter space relevant for the DJG potential. We therefore discard the image-charge term in equation (49) in the following, and consider henceforth

$$\beta V_{DJG2}(h) = \frac{16a\gamma_c\gamma_w}{\lambda_B}\mathrm{e}^{-\kappa(h-a)}. \tag{51}$$

For this potential we present in figure 11 the 10% error contour plot in the $(\kappa a, \kappa h)$ plane for various combinations of $\Phi_w$:$\Phi_c$. As is evident from this figure, the DJG potential becomes almost always tolerably good just provided that $\kappa a$ is sufficiently large. With increasing $\Phi_c$ the region with an error below 10% becomes larger, while it becomes smaller with increasing $\Phi_w$. $\Phi_w$:$\Phi_c \equiv 4$:2 produces the same error boundary as $\Phi_w$:$\Phi_c \equiv 3$:2.

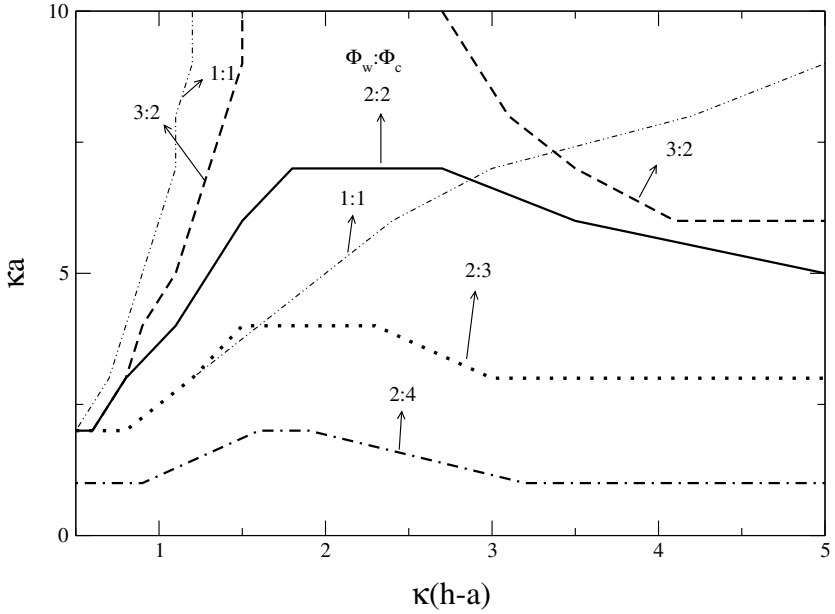


**Figure 11.** An error contour diagram as in figure 6 and figure 8, but now for the DJG potential, equation (51), for various combinations of $\Phi_w$:$\Phi_c$.

We have seen that $V_{GCH}(h)$ cannot be used if the colloidal surface potential is high and $\kappa a$ is at the same time large. But this is exactly the parameter regime where $\beta V_{DJG2}(h)$ performs exceedingly well. If one compares, for example, the $\Phi_w$:$\Phi_c \equiv 2$:2 error lines in figures 8 and 11, one can see that $V_{GCH}(h)$ and $\beta V_{DJG2}(h)$ are complementary in that $V_{GCH}(h)$ works for $\kappa a < 2$ while $\beta V_{DJG2}(h)$ is useful if $\kappa a$ is roughly greater than 5.

In summary, we have outlined the regions of validity of the three potentials $V_{St}(h)$, $V_{GCH}(h)$, and $\beta V_{DJG2}(h)$ using 10% error contour plots in figures 6, 8, and 11; this should be of use if one wishes to estimate the quality of one of the three potentials starting from a given set of input parameters ($\kappa a$, $\kappa h$, $\Phi_w$, $\Phi_c$). This we regard as the main result of this investigation.

### *4.2. A whole suspension of colloids: an interfacial Poisson–Boltzmann cell model*

So far we have considered the interaction between a single colloidal sphere and a wall. If this colloid is part of a concentrated suspension of colloids [46], things become different. We know, in fact, that in the bulk the effective colloid/colloid potentials may be strongly affected by the other colloids in the suspension (in particular in the case of low added salt [47]). As long as the mean distance $D$ between two colloids in the suspension is large compared to the thickness $\kappa^{-1}$ of the double layer around the colloid, one can expect pairwise-additive effective Yukawa potentials between two colloids. However, if $\kappa D$ becomes smaller than 1, the double layer around each colloid extends over a region in which there might be many other colloids.

This implies (i) that the colloids see each other as only partially screened particles, and (ii) that many colloids will interact with each other at the same time. It is still an open question how best to treat this complicated many-body problem theoretically [29].

A way commonly used to approximately determine the electrostatic potential inside a concentrated suspension of colloids is opened up by the so-called 'PB cell models' [49, 50]. These cell models rely on the assumption that every colloidal particle of the suspension experiences the same environment, which we know is strictly true only in the crystalline phase. Each colloid is assumed to be located at the centre of its cell, and all cells of the suspension have the same volume and shape. It therefore suffices to consider just one cell instead of the whole suspension and to calculate the electrostatic potential inside this cell only. The presence of the other (screened) colloids is taken into account by the appropriate choice of the boundary conditions for the PB equation. This constitutes a BVP whose solution provides us with the mean electrostatic potential inside the cell and thus the microionic density distribution. From it, one can then derive general thermodynamic quantities of the suspension, such as the osmotic pressure [51], or more specific quantities, such as the effective pair forces between the particles [48]. Such PB cell models have been used not only for colloids in suspensions [48, 51–55], but, more importantly, for suspensions of polyelectrolytes [50, 57], and also for a PB theory of swollen clay [56].

In regard to our problem of an interfacial colloid interacting with a wall, a PB cell model can also be useful for estimating the effect which the other colloids of the suspension may have on the interfacial colloid. In a recent paper, we suggested a PB cell model that is adapted to the interfacial geometry [58]. The cell of a colloid in the vicinity of the wall is now assumed to have the shape of a cylinder of radius $r_0$ and length $z_1$. $r_0$ is given by the volume of the cell, $V_{WS} = \pi r_0^2 z_1$, with the additional assumption that the cell has the same aspect ratio as a cube, $z_1 = 2r_0$. The macroion inside this cell has a variable position. At $z = 0$, the dielectric constant of the medium changes from $\epsilon'$ to $\epsilon$. No interfacial charges have been allowed for.

The BVP to study is similar to that of equation (2). The main difference is the appearance of two additional surfaces, due to the cell approximation, and thus of additional boundary conditions. These surfaces are (i) the curved surface of the cylinder and (ii) the straight side of the cylinder directed towards the bulk suspension. The boundary conditions follow from the assumption that the distance from any point on each of these two surfaces to the colloid in the centre of the cell is equal to the distance to any of the neighbouring colloids, so the normal component of the electric field at such a point must vanish for symmetry reasons (if the colloid is not in the centre of its cell, the boundary conditions become more complicated [58]). From the solution to this BVP one can then calculate the force acting on the colloid. Clearly, it is directed in the $z$-direction and we abbreviate its $z$-component as $F_z$. This force can most conveniently be obtained by integrating the stress tensor over the cell surface. It is given just by the difference $F(0) - F(z_1)$ between the forces which the colloid experiences from the two straight sides of the cylindrical cell. $F(0)$ ($F(z_1)$) here refers to the force coming from the side bordering the interface (bulk suspension).

Figure 12 shows this net force $F_z$ acting on the interfacial colloid as a function of the ratio of the dielectric constants of the substrate and the solution, $\epsilon'/\epsilon$, for various values of the reduced colloidal charge and the volume fraction of the suspension $\phi_{vol}$. The colloid is situated in the centre of its cell (other positions are considered in [58]). We see that, contrary to the case for a single interfacial colloid, the force acting on the colloid at this specific wall–colloid distance becomes *attractive*. This is so for all $\phi_{vol}$ and colloidal charges considered. The force is largest when the image charges vanish, i.e. when $\epsilon' = \epsilon$, and it is zero when $\epsilon' = 0$. The force increases with increasing $\epsilon'/\epsilon$, with increasing volume fraction, and with increasing colloidal charge.

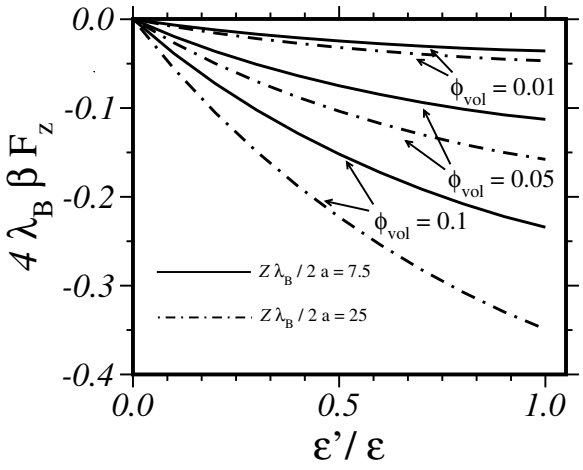


**Figure 12.** The total force acting on a colloid located at the centre of an interfacial cell for varying ratios of $\epsilon'/\epsilon$. The force is attractive and grows with increasing volume fraction $\phi_{vol}$ and scaled colloidal charge $Z\lambda_B/2a$.

This result is surprising only at first glance, and has a simple explanation. The ions inside the interfacial cell are exposed not only to the image charges from the region $z < 0$, but also to the (real!) charges of the neighbouring cell at $z > z_1$. These charges are taken into account implicitly by the boundary conditions. For all cases where $\epsilon' < \epsilon$, the image charges are not of the same magnitude as the original charges, but a little weaker—see equation (13)—and will thus exert a force on the colloid that is—though repulsive—not strong enough to balance the forces exerted from the corresponding ions in the cell at $z > z_1$. Therefore, the net force is attractive. As a result, the equilibrium position of the interfacial colloid is no longer at the centre position of its cell, but will be shifted towards the wall. Only in the case where $\epsilon'$ is zero do the image charges have the same magnitude as the original charges—equation (13)—and thus are able to match the charges from $z > z_1$: a totally symmetrical, bulklike situation is then recovered where there is no net force on the colloidal particle; see figure 12. A more systematic discussion of this effect can be found in [58], where we also calculated polarization surface charge densities at the wall and performed MC calculations to test the importance of finite-size effects.

In summary, we see that, when a whole suspension of colloids is considered, the repulsive forces which we have analysed for a single colloid next to a wall compete with the forces arising from all of the other colloids of the suspension. As we have seen, it can easily happen that the forces coming from the bulk colloids are stronger than the wall–colloid force, thus inducing a structural rearrangement of the colloidal suspension near a dielectric interface. We make this point in order to emphasize that the wall–colloid interaction potentials given in this article must be set in relation to the bulk colloid/colloid interaction if they are to be used to derive structural information on a colloidal suspension.

### *4.3. A single colloid near an interface: a TIRM experiment*

To demonstrate that the effective wall–colloid interaction potentials discussed in this paper can actually be observed in an experiment, we want to close this article by briefly reporting the results of a recent TIRM [8] experiment [60]. The experimental details will be reported elsewhere [60]; here we restrict ourselves to a rough sketch of the main idea of this experiment. A colloidal sphere (polystyrene; $a = 10\ \mu$m) of unknown negative surface charge density $\sigma_c$ is brought into a highly deionized (salt concentration in the $\mu$M regime) electrolytic suspension. Due to gravitation, the particle sinks to the bottom of the glass container, and is thus located in

the vicinity of a glass surface. This surface bears again an unknown amount of negative surface charge ($\sigma_w$), so there will be double layers both in front of the glass surface and surrounding the colloid. The colloid, being repelled by the repulsive double-layer forces and attracted by gravitation, will thus find a stable position at a finite distance from the glass interface, with small fluctuations in position due to Brownian forces.

When light is totally reflected at an interface, an evanescent field is created whose intensity $I$ decays exponentially with distance $z$ perpendicular to the interface, $I(z) = I_0 e^{-\beta z}$, with $\beta$ being the inverse penetration depth of the evanescent wave. What is important here is that $\beta$ is a quantity known *a priori*. The central idea of the TIRM method now is to measure the scattered intensity of the interfacial colloidal particle, which is located in this evanescent wave, and to deduce the wall–colloid distance from the measured intensity through the known relation $I(z) = I_0 e^{-\beta z}$. In order to obtain the spatial dependence of the potential energy of the particle, one has to measure the separation distances sampled by the colloidal sphere for a statistically long period of time. From this, the probability of finding the particle at any separation distance can be calculated; it is related to the potential energy via the Boltzmann distribution. This potential energy is the sum of the gravitational and double-layer potentials. Figure 13 shows the measured potentials for ten different salt concentrations (10 nm $< \kappa^{-1} <$ 100 nm) when the gravitational contribution is subtracted. Thus, figure 13 represents a direct experimental observation of what we have discussed in this article: the effective wall–colloid potentials due to double-layer forces.

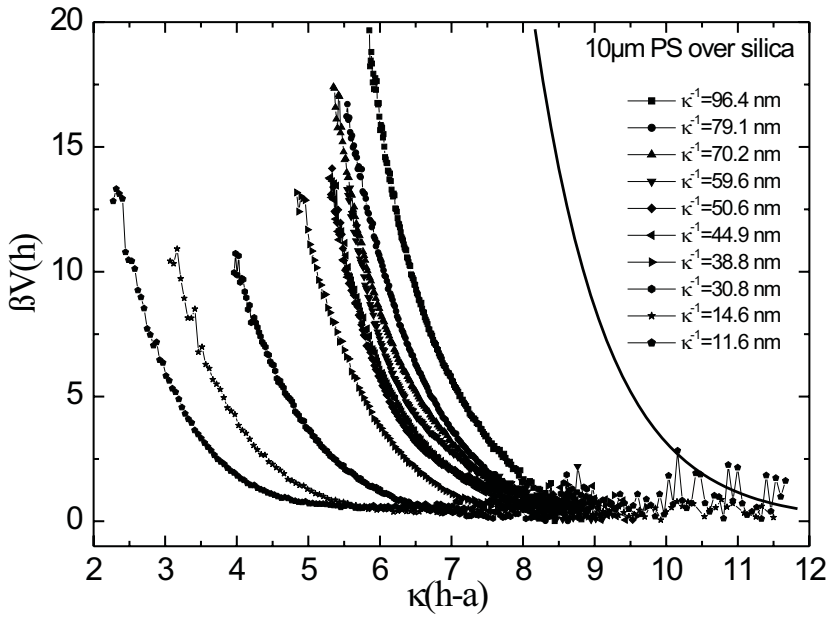


**Figure 13.** Effective double-layer potentials between a glass surface and a colloidal sphere, experimentally determined for various salt concentrations using the TIRM method [60]. The function $16ae^{-\kappa(h-a)}/\lambda_B$ is plotted as solid line.

To find out which of the approximate potentials, equation (48) or equation (51), is appropriate for this experiment, we need to specify the surface potentials using equation (45), which however is possible only if we know the surface densities $\sigma_c$, $\sigma_w$. In reference [60], we explain how to use such salt-dependent measurements of double-layer forces to determine

surface densities. We find that $\Phi_w$ and $\Phi_c$ are both of the order of one. While these values lie within the range studied theoretically here, the values of $\kappa a$ are not. The double layers in our experiment were extremely thin, with values of $\kappa a$ ranging between 50 and 500, which is far beyond the range studied in figures 8 and 11. Such high values of $\kappa a$ cannot be calculated with our numerical scheme for solving the PB equation, and one thus depends on extrapolating a sequence of error curves for increasing $\kappa a$. The general trend of figure 11 suggests that since the DJG potential in equation (51) seems to work for every combination of $\Phi_w$:$\Phi_c$ just as long as the $\kappa a$-value is large enough, the agreement with the PB theory should become better as the $\kappa a$-value becomes larger . This is indeed the case, as we have shown in reference [60] for a set of parameters adapted to the experimental conditions. The calculation shows that the potential of equation (51), $\beta V(h) = 16a\gamma_c\gamma_w \mathrm{e}^{-\kappa(h-a)}/\lambda_B$, should be almost identical to the full mean-field result in the parameter regime under consideration. As for the image-charge contribution, we found that it becomes less important as $\kappa a$ becomes higher, and figure 10 shows that at $\kappa a = 10.0$ the image-charge contribution for $\Phi_w$:$\Phi_c = 1$:1 already has a rather small effect in the distance regime explored experimentally ($\kappa(h - a) > 2$). Thus in our experiment with $\kappa a > 50$, the colloid is too large and too far away from the surface to be sensitive to image-charge repulsion.

Recalling that the $\gamma$-factors in this potential still depend on the salt concentration—see equation (46)—we now understand that the salt dependence of the interaction potentials observed in figure 13 comes in through the product $\gamma_w\gamma_c$ in the interaction potential. Given the values of $\sigma_w$ and $\sigma_c$, we can determine $\gamma_w\gamma_c$ for all measured salt concentrations. Dividing each experimentally determined potential in figure 14 by its value of $\gamma_w\gamma_c$, we see (in figure 14) all ten potential curves collapsing onto one master curve (solid line), which is just the function $\beta V(h)/\gamma_c\gamma_w = 16a\mathrm{e}^{-\kappa(h-a)}/\lambda_B$. The agreement is remarkably good and demonstrates very nicely that and how precisely the wall–colloid interaction potential of equation (51) can be measured experimentally.

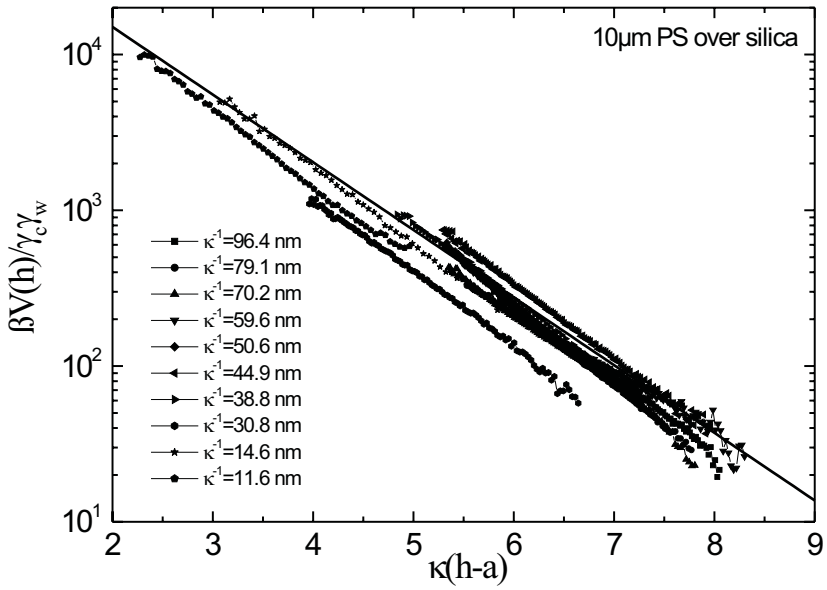


**Figure 14.** The potentials of figure 13 divided by $\gamma_w\gamma_c$ all collapse onto the simple function $16a\mathrm{e}^{-\kappa(h-a)}/\lambda_B$, shown as a line in this logarithmic plot.

## 5. Conclusions

We have been concerned with the question of how a charged sphere inside an electrolytic solution of dielectric constant $\epsilon$ interacts with a charged wall of dielectric constant $\epsilon'$. We first considered the colloidal sphere as a point charge, and discussed its interaction with both an uncharged and a charged wall. Renormalizing the charge by a factor $g_h$, one can afterwards correct these interaction potentials to account for the finite size of the colloidal sphere. Starting from these linear potentials, we arrived at two potentials, approximately valid also in the non-linear regime: equation (48) (GCH potential) and equation (49) (DJG potential). The range of validity of these potentials was then checked by comparing them with the numerical solution to the full PB equation. We may summarize the main points of this paper as follows:

- For an uncharged wall of dielectric constant $\epsilon'$, the effective wall–colloid potential is repulsive if $\epsilon'/\epsilon \to 0$ and attractive if $\epsilon/\epsilon' \to 0$. A charged colloid in an aqueous suspension will therefore be repelled from an air/water interface, and attracted to a metal/water interface. In contrast to what was said in [11] and [31], there is no electrostatic attraction of colloids to an air/water interface.
- Even if there are no images charges present ($\epsilon' = \epsilon$), a colloid is still repelled from an uncharged interface due to a confinement effect.
- The $h$-dependent renormalization factor $g_h$ is found to be only a few per cent different from $g_\infty$.
- In linear theory and if $\epsilon'/\epsilon \to 0$, the interaction of a colloid of finite size with an uncharged wall is just half of the usual repulsive Yukawa potential of DLVO theory between two like-charged spheres (see $\beta V_{St}(h)$ of equation (32)), where one sphere is the screened colloid at $z = h$ and the other, being located at $z = -h$, represents nothing but the screened image of the colloid. Then only the factor $1/2$ in the potential remains as a reminder of the fact that we are concerned not with a colloid/colloid interaction, but with a colloid/wall interaction.
- One can reuse Stillinger's potential for a point charge near an uncharged wall as the Green's function for the linearized Poisson–Boltzmann equation for the case of an arbitrary distribution of fixed charges. Using the point-charge approximation, the effective potential is then a sum of the potential for an uncharged wall and the interaction of the colloid with the unperturbed double layer of the wall.
- We checked the validity of $\beta V_{st}(h)$ for the uncharged wall and found that it produces an error below 10% for all values of $\kappa a$ as long as $\kappa(h-a) > 0.61$ and $\Phi_c \leqslant 1$.
- Adding to $\beta V_{st}(h)$ the interaction energy of a renormalized point charge $Z/g_\infty$ in the unperturbed Gouy–Chapman layer, we arrive at the GCH potential, equation (48), which we have found to be appropriate for all $\kappa a$ provided that $\kappa(h-a) > 2$ and $\Phi_c \leqslant 1$, in accord with the range of validity found for $\beta V_{st}(h)$ alone. We have explicitly checked that inclusion of the image-charge contribution improves the accuracy.
- If $\Phi_c > 1$, the DJG potential, equation (49), without image-charge contributions is almost always tolerably good for all $\kappa(h-a)$ provided only that $\kappa a$ is sufficiently large (error below 10% if $\kappa a > 6$ for $\Phi_w{:}\Phi_c \equiv 2{:}2$). With increasing $\Phi_c$ this region with error below 10% becomes larger, while it becomes smaller with increasing $\Phi_w$.
- When a suspension of colloids is considered, we need to be aware of the fact that the wall–colloid interaction potential must be set in relation to the bulk colloid/colloid interaction potential. The latter is the one that is more repulsive in the case of an uncharged wall with $\epsilon'/\epsilon > 0$. The equilibrium position of the interfacial colloid in its cell is therefore slightly shifted towards the wall.

- We performed a TIRM experiment to measure the effective wall–colloid potential and found a nice agreement of the DJG potential and the experimental data, with the colloidal surface charge density being the only open parameter.

## Appendix A. Solution of the Poisson–Boltzmann equation in bispherical coordinates

We aim to explain here in some detail the procedures followed in solving the PB BVP stated in equation (2) for $\phi$ with constant-charge boundary conditions. Scaling all lengths by $\kappa^{-1}$ and introducing

$$\begin{aligned} \Sigma_w &= \lambda_B \sigma_w / \kappa \\ \Sigma_c &= \lambda_B \sigma_c / \kappa \end{aligned} \tag{A.1}$$

the BVP of equation (2) for the special case $\epsilon' = 0$ can be written in the following form:

$$\begin{aligned} \nabla^2 \phi &= \sinh \phi && \vec{r} \in G \\ \vec{n}_w \nabla \phi &= 4\pi \Sigma_w && \vec{r} \in \partial G_w \\ \vec{n}_c \nabla \phi &= 4\pi \Sigma_c && \vec{r} \in \partial G_c \\ \phi &= 0 && \vec{r} \to \infty. \end{aligned} \tag{A.2}$$

In the absence of any charged body (e.g. the colloid) in the electrolyte, this BVP is solved by the Gouy–Chapman potential $\phi^{GC}$ given in equations (44) and (45). We define the potential $\tilde{\phi}$ as the difference of the true potential $\phi$ and $\phi^{GC}$ which leads to a new BVP in $\phi^{GC}$ and $\tilde{\phi}$ as follows:

$$\begin{aligned} \nabla^2 \tilde{\phi} &= \sinh(\tilde{\phi} + \phi^{GC}) - \sinh \phi^{GC} && \vec{r} \in G \\ \vec{n}_w \nabla \tilde{\phi} &= 0 && \vec{r} \in \partial G_w \\ \vec{n}_c \nabla \tilde{\phi} &= 4\pi \Sigma_c - \vec{n}_c \nabla \phi^{GC} && \vec{r} \in \partial G_c \\ \tilde{\phi}(\infty) &= 0 && \vec{r} \to \infty. \end{aligned} \tag{A.3}$$

We thus calculate not the double layer in front of the wall, but its perturbation due to the charged colloid, a trick which has primarily computational advantages. It would be even better if we could also subtract the spherical double layer around the isolated sphere, but this is not established as being appropriate analytically. For purposes of achieving good accuracy in the numerical scheme, we now solve this BVP in bispherical coordinates [59] (bsc) $(\eta, \theta)$, as has been done by others before [21, 41, 42].

In the bsc system, the region external to the spheres (colloid and colloid image) is the rectangular domain (figure A1): $-\eta_0 \leqslant \eta \leqslant \eta_0$ and $0 \leqslant \theta \leqslant \pi$, while the regions in the interior of the sphere correspond to the following domains: (i) colloid image: $-\infty \leqslant \eta \leqslant -\eta_0$ and $0 \leqslant \theta \leqslant \pi$; (ii) real colloid: $\eta_0 \leqslant \eta \leqslant \infty$ and $0 \leqslant \theta \leqslant \pi$. Since the spheres are of the same size, it is sufficient to consider the real half-space, i.e. the rectangular domain $0 \leqslant \eta \leqslant \eta_0$ and $0 \leqslant \theta \leqslant \pi$.

The bsc are related to the cylindrical coordinates $(\kappa\varrho, \kappa z)$, where $z$ is the component normal to the wall and $\varrho$ $(=\sqrt{x^2 + y^2})$ is the radial part:

$$\begin{aligned} z &= \frac{b \sinh \eta}{\cosh \eta - \cos \theta} \\ \varrho &= \frac{b \sin \theta}{\cosh \eta - \cos \theta}. \end{aligned} \tag{A.4}$$

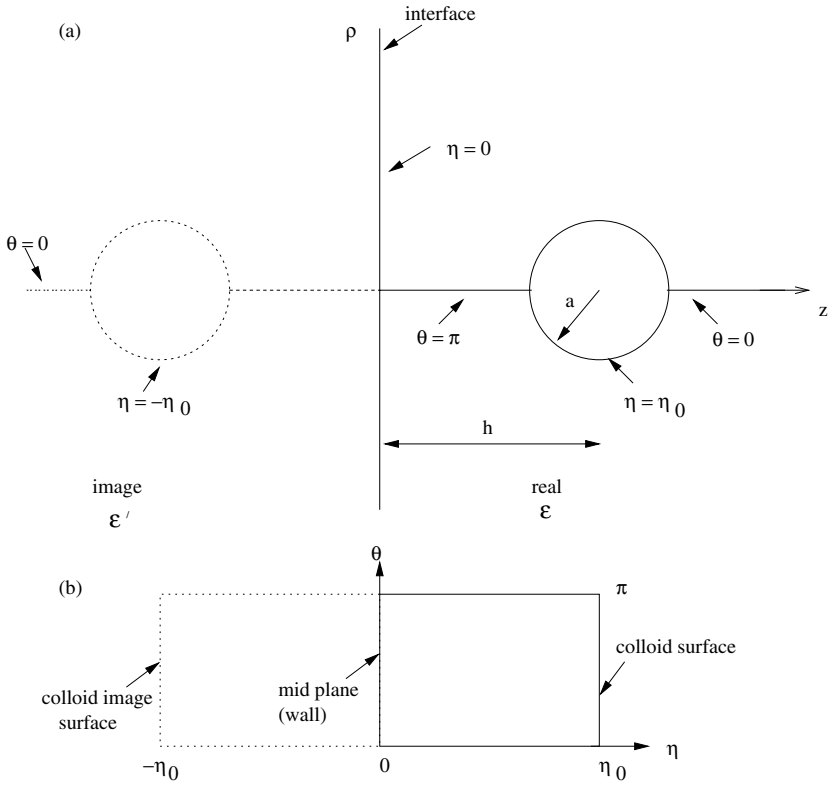


**Figure A1.** The advantage of using bispherical coordinates: the region exterior to both spheres in (a) becomes a rectangle in the $(\eta, \theta)$ plane in (b).

The regions of constant $\eta$ are spheres of radius $R_\eta$; their centres are at a distance $C_\eta$:

$$\begin{aligned} R_\eta &= \frac{\kappa b}{\sinh \eta} \\ C_\eta &= \frac{\kappa b \cosh \eta}{\sinh \eta} = \kappa b \coth \eta. \end{aligned} \tag{A.5}$$

The constants $b$ and $\eta_0$ are then defined by requiring that $R_{\eta_0} = \kappa a$ and $C_{\eta_0} = \kappa h$. We can now write the BVP in equation (A.3) in terms of $(\eta, \theta)$ coordinates by expressing the Laplacian in bsc [59] and using the boundary conditions for $\tilde{\phi}$ on the four sides of the rectangle (see figure A1(b)) as follows:

$$\begin{aligned} &\partial_\eta \tilde{\phi}\big|_{\eta=\eta_0} = 2\kappa b \sinh(\Phi_W/2) \frac{1 - \cosh \eta_0 \cos \theta}{(\cosh \eta_0 - \cos \theta)^2} - \frac{4\pi \kappa b \Sigma_c}{(\cosh \eta_0 - \cos \theta)} \\ &\partial_\eta \tilde{\phi}\big|_{\eta=0} = \partial_\theta \tilde{\phi}\big|_{\theta=\pi} = \partial_\theta \tilde{\phi}\big|_{\theta=0} = \tilde{\phi}(\eta = 0, \theta = 0) = 0. \end{aligned} \tag{A.6}$$

For the new BVP we now employ the Newton–Raphson iteration scheme, which takes the form

$$\nabla^2 \tilde{\phi}_{n+1} - \cosh(\tilde{\phi}_n + \phi^{GC}) \tilde{\phi}_{n+1} = \sinh(\tilde{\phi}_n + \phi^{GC}) - \sinh \phi^{GC} - \cosh(\tilde{\phi}_n + \phi^{GC}) \tilde{\phi}_n \tag{A.7}$$

where a new estimate $\tilde{\phi}_{n+1}$ of the solution of the non-linear PB equation is obtained from a previous estimate, $\phi_n$.

## Appendix B. Force via the stress tensor

The force $\vec{F}$ acting on a particle enclosed by a surface $S$ can be calculated by integrating the stress tensor $\vec{\vec{T}}$:

$$\vec{F} = \int_S \mathrm{d}S\ \vec{\vec{T}} \cdot \vec{n} \tag{B.1}$$

where $\vec{n}$ is a unit normal pointing into the surface. Here the total stress tensor is the sum of an osmotic pressure term and a Maxwell stress

$$\vec{\vec{T}} = \left(\Pi + \frac{\epsilon}{8\pi}\mathcal{E}^2\right)\vec{\vec{I}} - \frac{\epsilon}{4\pi}\vec{\mathcal{E}}\vec{\mathcal{E}}. \tag{B.2}$$

$\vec{\mathcal{E}}$ is the electric field, $\vec{\vec{I}}$ is a unit tensor, and $\Pi$ is the difference in local osmotic pressure from that in the bulk electrolyte:

$$\beta\Pi = (\rho_+ + \rho_- - 2c_s) = 2c_s(\cosh\phi - 1) \tag{B.3}$$

where $\rho_\pm = c_s \mathrm{e}^{\mp\phi}$ ($c_s$ is the bulk concentration). Rewriting the stress tensor in scaled units ($\vec{E} = e\beta\vec{\mathcal{E}}$) we have

$$\beta\vec{\vec{T}} = 2c_s(\cosh\phi - 1) + \frac{1}{8\pi\lambda_B}\left[E^2\vec{\vec{I}} - 2\vec{E}\,\vec{E}\right]. \tag{B.4}$$

Since the system is symmetrical about the axis, $z$, joining the centres of the particle and the particle image (colloid/colloid image) (see figure A1), the direction of the force on the particle is normal to the wall, i.e.

$$\beta F_z = \int_{S_{\eta_c}} \mathrm{d}S_{\eta_c}\ \vec{e}_z \cdot \beta\vec{\vec{T}} \cdot \vec{n}. \tag{B.5}$$

The enclosing surface $S_{\eta_c}$ is an $\eta$-coordinate surface ($0 \leqslant \eta_c \leqslant \eta_0$). $\vec{n}$ is then a vector normal to the $\eta_c$-coordinate surface, $\vec{n} = \vec{e}_\eta$, where $\vec{e}_\eta$ and $\vec{e}_\theta$ are the unit vectors in the bsc system:

$$\begin{aligned}\vec{e}_\eta &= \frac{\partial_\eta\vec{r}}{|\partial_\eta\vec{r}|}\\ \vec{e}_\theta &= \frac{\partial_\theta\vec{r}}{|\partial_\theta\vec{r}|}\end{aligned} \tag{B.6}$$

with $\vec{r} = z(\eta,\theta)\vec{e}_z + \varrho(\eta,\theta)\vec{e}_\varrho$ from equation (A.4). Therefore,

$$\vec{e}_z \cdot \vec{\vec{T}} \cdot \vec{n} = \vec{e}_z \cdot \vec{\vec{T}} \cdot \vec{e}_\eta = T_{\eta\eta}\,\vec{e}_z \cdot \vec{e}_\eta + T_{\theta\eta}\,\vec{e}_z \cdot \vec{e}_\theta \tag{B.7}$$

and

$$\begin{aligned}\vec{e}_\eta \cdot \vec{e}_z &= \frac{1 - \cosh\eta\cos\theta}{\cosh\eta - \cos\theta}\\ \vec{e}_\theta \cdot \vec{e}_z &= -\left(\frac{\sinh\eta\sin\theta}{\cosh\eta - \cos\theta}\right).\end{aligned} \tag{B.8}$$

With

$$\int \mathrm{d}S_{\eta_c} = \int 2\pi\,\frac{(\kappa b)^2\sin\theta}{(\cosh\eta_c - \cos\theta)^2}\,\mathrm{d}\theta \tag{B.9}$$

equation (B.5) then becomes

$$\begin{aligned}\beta F_z = 2\pi\int_0^\pi \Bigg\{&\left[2c_s(\cosh\phi - 1) + \frac{1}{8\pi\lambda_B}(E_\theta^2 - E_\eta^2)\right]\frac{1 - \cosh\eta_c\cos\theta}{\cosh\eta_c - \cos\theta}\\ &+ \left[\frac{1}{4\pi\lambda_B}E_\eta E_\theta\right]\frac{\sinh\eta_c\sin\theta}{\cosh\eta_c - \cosh\theta}\Bigg\}\frac{(\kappa b)^2\sin\theta}{(\cosh\eta_c - \cos\theta)^2}\ \mathrm{d}\theta.\end{aligned} \tag{B.10}$$

Recalling that $c_s = \kappa^2/8\pi\lambda_B$ and choosing the enclosing surface $S_{\eta_c}$ to be the interfacial wall corresponding to $\eta_c = 0$, the dimensionless force $f = 4\pi\lambda_B\beta F_z$ takes the form

$$f = \pi \int_0^\pi \mathrm{d}\theta \, \left[2\kappa^2(\cosh\phi - 1) + E_\theta^2 - E_\eta^2\right] \frac{(\kappa b)^2 \sin\theta}{(1-\cos\theta)^2}. \tag{B.11}$$

The electric field $E_{\eta/\theta}$ can be written in terms of $\phi$:

$$bE_\eta = (1-\cos\theta)\,\partial_\eta\phi \qquad bE_\theta = (1-\cos\theta)\,\partial_\theta\phi$$

and substituting this in equation (B.11) we finally write the reduced force as

$$f = \pi \int_0^\pi \mathrm{d}\theta \left(\frac{2(\kappa b)^2 \sin\theta}{(1-\cos\theta)^2}(\cosh\phi - 1) + \left[\partial_\theta\phi^2 - \partial_\eta\phi^2\right]\sin\theta\right)_{\eta=\eta_c=0}. \tag{B.12}$$

Noting that $\partial_\eta\phi$ at $\eta = 0$ is known from our boundary condition, we have that

$$\partial_\eta\phi^2\big|_{\eta=0} = (\partial_\eta\phi^{GC})^2\big|_{\eta=0} = \left(\frac{2\kappa b}{1-\cos\theta}\right)^2 \sinh^2\Phi_w/2 = \left(\frac{2\kappa b}{1-\cos\theta}\right)^2 \frac{1}{2}(\cosh(\Phi_w) - 1) \tag{B.13}$$

and we can simplify equation (B.12) to

$$f = \pi \int_0^\pi \mathrm{d}\theta \left(\frac{2(\kappa a \sinh\eta_0)^2 \sin\theta}{(1-\cos\theta)^2}[\cosh\phi - \cosh\Phi_w] + \left(\frac{\partial\phi}{\partial\theta}\right)^2 \sin\theta\right)_{\eta=0}. \tag{B.14}$$

This force can easily be calculated once $\phi$ is known. All of the error estimates of the analytical potentials made in this paper were made on the basis of forces. If potentials are plotted, we have obtained them from numerically integrating the calculated forces.

## References


[1] Russel W B, Saville D A and Schowalter W R 1989 *Colloidal Dispersions* (Cambridge: Cambridge University Press)

[2] Löwen H and Hansen J-P 2000 *Annu. Rev. Phys. Chem.* **51** 209

[3] Kepler G M and Fraden S 1994 *Phys. Rev. Lett.* **73** 356
Crocker J C and Grier D G 1996 *Phys. Rev. Lett.* **77** 1897
Grier D G 1998 *Nature* **393** 621
Larsen A M and Grier D G 1997 *Nature* **385** 230
Carbajal-Tinoco M D, Cruz de León G and Arauz-Lara J L 1997 *Phys. Rev.* E **56** 6962
Cruz de León G and Arauz-Lara J L 1999 *Phys. Rev.* E **59** 4203

[4] Goulding E D and Hansen J-P 1999 *Europhys. Lett.* **46** 407
Bowen W R and Sharif A O 1998 *Nature* **393** 663
Neu J C 1999 *Phys. Rev. Lett.* **82** 1072
Allahyarov E, D'Amico I and Löwen H 1999 *Phys. Rev.* E **60** 3199
Sader J E and Chan D Y C 1999 *J. Colloid Interface Sci.* **213** 268
Sader J E and Chan D Y C 2000 *Langmuir* **16** 324
Trizac E and Raimbault J L 1999 *Phys. Rev.* E **60** 6530
Allahyarov E, D'Amico I and Löwen H 1998 *Phys. Rev. Lett.* **81** 1334
Goulding D and Hansen J-P 1998 *Mol. Phys.* **95** 649

[5] Dufresne E R, Squires T M, Brenner M P and Grier D G 2000 *Phys. Rev. Lett.* **85** 3317

[6] Firshein W 1989 *Annu. Rev. Microbiol.* **43** 89
Verma I M and Somia N 1997 *Nature* **389** 239
Behr J P 1994 *Bioconjugate Chem.* **5** 382
Maier B and Rädler J O 1999 *Phys. Rev. Lett.* **82** 1911
Rädler J O, Koltover I, Salditt T and Safinya C R 1997 *Science* **275** 810
Sladitt T, Koltover I, Rädler J and Safinya C R 1997 *Phys. Rev. Lett.* **79** 2582
Wagner K, Harris D, May S, Kahl V, Rädler J O and Ben-Shaul A 2000 *Langmuir* **26** 303

[7] Sens P and Joanny J F 2000 *Phys. Rev. Lett.* **84** 4862

[8] Prieve D C, Luo F and Lanni F 1987 *Faraday Discuss. Chem. Soc.* **83** 297
Walz J Y 1997 *Curr. Opin. Colloid Interface Sci.* **2** 600
Prieve D C, Bike S G and Frej N A 1990 *Faraday Discuss. Chem. Soc.* **90** 209
Prieve D C and Frej N A 1990 *Langmuir* **6** 396
Bike S G and Prieve D C 1990 *Int. J. Multiphase Flow* **16** 727
Brown M A and Staples E J 1990 *Langmuir* **6** 1260
[9] Israelachvili J 1992 *Intermolecular and Surface Forces* 2nd edn (London: Academic)
[10] Robertson S K, Uhrick A F and Bike S G 1998 *J. Colloid Interface Sci.* **202** 208
[11] Earnshaw J C 1986 *J. Phys. D: Appl. Phys.* **19** 1863
Haughey D and Earnshaw J C 1996 *Colloids Surf.* A **106** 237
Hurd A J 1985 *J. Phys. A: Math. Gen.* **18** 1055
[12] Van Blaaderen A and Wiltzius P 1995 *Science* **270** 1177
[13] Grier D G and Murray C A 1991 *J. Chem. Phys.* **100** 9088
[14] Onoda G Y 1985 *Phys. Rev. Lett.* **55** 226
[15] Tandon S, Kesavamoorthy R and Asher S A 1998 *J. Chem. Phys.* **109** 6490
Kesavamoorthy R, Rajalakshmi M and Balu Rao C 1989 *J. Phys.: Condens. Matter* **1** 7149
Kesavamoorthy R, Balu Rao C and Tata B V R 1991 *J. Phys.: Condens. Matter* **3** 7973
[16] Forsten K E, Kozack R E, Lauffenburger D A and Subramaniam S 1994 *J. Phys. Chem.* **98** 5580
[17] Hurd A J and Schaefer D J 1985 *Phys. Rev. Lett.* **54** 1043
[18] Pieranski P 1980 *Phys. Rev. Lett.* **45** 569
[19] Carnie S L and Chan D Y C 1993 *J. Colloid Interface Sci.* **155** 297
[20] Carnie S L and Chan D Y C 1993 *J. Colloid Interface Sci.* **161** 260
[21] Carnie S L, Chan D Y C and Stankovich J 1994 *J. Colloid Interface Sci.* **165** 116
[22] Carnie S L, Chan D Y C and Gunning J S 1994 *Langmuir* **10** 2993
[23] Stankovich J and Carnie S L 1996 *Langmuir* **12** 1453
[24] Sader J E, Carnie S L and Chan D Y 1995 *J. Colloid Interface Sci.* **171** 46
[25] Warszynski P and Adamczyk Z 1997 *J. Colloid Interface Sci.* **187** 283
[26] Bhattacharjee S and Elimelech M 1997 *J. Colloid Interface Sci.* **193** 273
[27] Verwey E J W and Overbeek J T G 1948 *Theory of the Stability of Lyophobic Colloids* (Amsterdam: Elsevier)
[28] Belloni L 1998 *Colloids Surf.* A **140** 227
[29] Belloni L 2000 *J. Phys.: Condens. Matter* **12** R549
[30] Barrat J L and Joanny J F 1996 *Adv. Chem. Phys.* **94** 1
[31] Stillinger F H 1961 *J. Chem. Phys.* **35** 1584
[32] Schmutzer E 1955 *Z. Phys. Chem.* **204** 131
[33] Durand E 1966 *Electrostatique* vol III (Paris: Masson)
[34] Netz R R 1999 *Phys. Rev.* E **60** 3174
[35] Carnie S L and Torrie G M 1987 *Adv. Chem. Phys.* **56** 141
[36] Martynov G A 1966 *Research in Surface Forces* vol 2, ed B V Derjaguin (New York: Consultants Bureau) pp 75, 84, 94
[37] Nicholls A L III and Pratt L R 1982 *J. Chem. Phys.* **76** 3782
[38] Wagner C 1924 *Z. Phys.* **25** 474
[39] Onsager L and Samaras N N T 1934 *J. Chem. Phys.* **2** 528
[40] Palkar S A and Lenhoff A M 1994 *J. Colloid Interface Sci.* **165** 177
[41] Ledbetter J E, Croxton T L and McQuarrie D A 1981 *Can. J. Chem.* **59** 1860
[42] McCartney L N and Levine S J 1969 *J. Colloid Interface Sci.* **30** 345
[43] Bell G M, Levine S and McCartney L N 1970 *J. Colloid Interface Sci.* **33** 335
[44] Evans D F and Wennerström H 1994 *The Colloidal Domain: Where Physics, Chemistry, Biology and Technology Meet* (New York: VCH)
[45] Glendinning A B and Russel W B 1983 *J. Colloid Interface Sci.* **93** 95
[46] Nägele G 1996 *Phys. Rep.* **272** 215
[47] Beresford-Smith B, Chan D Y and Mitchell D J 1984 *J. Colloid Interface Sci.* **105** 216
[48] von Grünberg H H and Belloni L 2000 *Phys. Rev.* E **62** 2493
[49] Hill T L 1960 *Statistical Mechanics* (Reading, MA: Addison-Wesley)
[50] Wennerström H, Jönsson B and Linse P 1982 *J. Chem. Phys.* **76** 4665
[51] Alexander S, Chaikin P M, Grant P, Morales G J, Pincus P and Hone D 1984 *J. Chem. Phys.* **80** 5776
[52] Groot R D 1991 *J. Chem. Phys.* **95** 9191
[53] Gisler T, Schulz S F, Borkovec M, Sticher H, Schurtenberger P, D'Aguanno B and Klein R 1994 *J. Chem. Phys.* **101** 9924

[54] Stevens M J, Falk M L and Robbins M O 1996 *J. Chem. Phys.* **104** 5209
[55] von Grünberg H H 2000 *J. Phys.: Condens. Matter* **12** 6039
[56] Leote de Carvalho R J F, Trizac E and Hansen J-P 1998 *Europhys. Lett.* **43** 369
[57] Alfrey T, Berg P and Morawetz H J 1951 *J. Polym. Sci.* **7** 543
Fuoss R M, Katchalsky A and Lipson S 1951 *Proc. Natl Acad. Sci. USA* **37** 579
le Bret M and Zimm B H 1984 *Biopolymers* **23** 287
[58] von Grünberg H H and Mbamala E C 2000 *J. Phys.: Condens. Matter* **12**
[59] Moon P and Spencer D E 1971 *Field Theory Handbook* 2dn edn (Berlin: Springer) p 110
[60] von Grünberg H H, Helden L, Leiderer P and Bechinger C 2001 *J. Chem. Phys.* at press